Cryo-EM structures of inactive and G_i-coupled $GABA_B$ heterodimer

Chunyou Mao[1,2,3]*, Cangsong Shen[4,5]*, Chuntao Li[5], Dan-Dan Shen[1,2,3], Chanjuan Xu[4.7], Shenglan Zhang[4,7], Rui Zhou[4], Qingya Shen[1,2,3], Li-Nan Chen[5], Zhinong Jiang[6], Jianfeng Liu[4,7,#], Yan Zhang[1,2,3,#]

Affiliations:

[1] Department of Pathology of Sir Run Run Shaw Hospital, and Department of Biophysics, Zhejiang University School of Medicine, Hangzhou 310058, China.

[2] MOE Frontier Science Center for Brain Research and Brain–Machine Integration, Zhejiang University School of Medicine, Hangzhou 310058, China.

[3] Key Laboratory of Immunity and Inflammatory Diseases of Zhejiang Province, Hangzhou 310058, China.

[4] Key Laboratory of Molecular Biophysics of MOE, International Research Center for Sensory Biology and Technology of MOST, School of Life Science and Technology, Huazhong University of Science and Technology, Wuhan 430074, China.

[5] Department of Biophysics, Zhejiang University School of Medicine, Hangzhou 310058, China.

[6] Department of Pathology of Sir Run Run Shaw Hospital, Zhejiang University School of Medicine, Hangzhou 310058, China.

[7] Guangzhou Regenerative Medicine and Health Guangdong Laboratory, Guangzhou 510005, China.

* These authors contributed equally to this work.

Co-corresponding authors: Yan Zhang (zhang_yan@zju.edu.cn); Jianfeng Liu (jfliu@mail.hust.edu.cn)

Abstract

Metabotropic $GABA_B$ G protein-coupled receptor functions as a mandatory heterodimer of GB1 and GB2 subunits and mediates inhibitory neurotransmission in the central nervous system. Each subunit is composed of the extracellular Venus flytrap (VFT) domain and transmembrane (TM) domain. Here we present cryo-EM structures of human full-length heterodimeric $GABA_B$ receptor in the antagonist-bound inactive state and in the active state complexed with agonist and positive allosteric modulator in the presence of G_{i1} protein at a resolution range of 2.8-3.0 Å. Cryo-EM analysis of the activated-$GABA_B$–G_{i1} complex revealed that G_{i1} couples to the activated receptor primarily in three major conformations, one via GB1 TM and two via GB2 TM, respectively. Our structures reveal that agonist binding stabilizes the closure of GB1 VFT, which in turn triggers a rearrangement of TM interfaces between two subunits from TM3-

33 TM5/TM3-TM5 in the inactive state to TM6/TM6 in the active state and finally induces the
34 opening of intracellular loop 3 and synergistically shifting of TM3, 4 and 5 helices in GB2 TM
35 domain to accommodate the α5-helix of G_{i1}. These results provide a structural framework for
36 understanding class C GPCR activation and a rational template for allosteric modulator design
37 targeting dimeric interface of $GABA_B$ receptor.

38

39 **Introduction**

40 Metabotropic $GABA_B$ receptor is a G protein-coupled receptor (GPCR) for the major
41 inhibitory neurotransmitter, γ-amino butyric acid (GABA), in the central nervous system to
42 mediate slow and prolonged inhibitory activity[1-3]. $GABA_B$ receptor couples to $G_{i/o}$ proteins to
43 inhibit neurotransmitter release in pre-synaptic neurons and cause hyperpolarization in the post-
44 synaptic neurons[4]. $GABA_B$ receptor suppresses adenylyl cyclase through $G\alpha_{i/o}$, while gating ion
45 channels and transactivating receptor tyrosine kinases via $G\beta\gamma$[5-8]. Dysfunctions of $GABA_B$
46 receptor or mutation in its genes have been implicated in a variety of neurological and
47 psychiatric disorders including epilepsy, pain, anxiety, depression, schizophrenia, drug
48 addiction, Rett syndrome and epileptic encephalopathies[4,9]. Recent studies reveal that the auto-
49 antibodies of $GABA_B$ receptor are possibly the origin of epilepsies and encephalitis[10,11].
50 Although a large number of antagonists and agonists and positive or negative allosteric
51 modulators (PAMs or NAMs) have been developed for $GABA_B$ receptor[12], only two agonists
52 approved as therapeutic drugs: baclofen (Lioresal®) used for the treatment of muscle spasticity
53 and alcohol addiction[13,14] and γ-hydroxybutyrate (GHB) used for the treatment of narcolepsy[15].

54 $GABA_B$ receptor belongs to the class C GPCR composed by metabotropic glutamate
55 receptors (mGlus), calcium-sensing receptor (CaSR) and taste 1 receptors[16]. Class C GPCR
56 form obligatory dimers, among them, mGlus and CaSR form the homodimer[17,18], whereas
57 $GABA_B$ receptor is an obligatory heterodimer of two subunits $GABA_{B1}$ (GB1) and $GABA_{B2}$
58 (GB2)[19,20]. Each subunit is composed of a large extracellular 'Venus Flytrap' (VFT) domain, a
59 transmembrane (TM) domain, and a cytoplasmic tail[21] (Extended Data Fig. 1a, b). GB1
60 possesses an endoplasmic reticulum (ER) retention motif in its cytoplasmic tail[22]. The

interaction between GB1 and GB2 facilitates its cell surface expression through coiled-coil interactions in its cytoplasmic tail[23]. While GB1 is responsible for ligand recognition through its VFT[24], GB2 couples $G_{i/o}$ proteins through its TM[25,26]. However, a line of evidence show that in the absence of GB2, $GB1_{asa}$ (a GB1 mutant with deletion of ER retention signal) at the cell surface or ER-localized GB1 also induces downstream signaling through $G_{i/o}$ proteins[27,28].

The crystal structures of isolated heterodimeric VFT of $GABA_B$ receptor in presence of the antagonist or agonist revealed the open or closed conformation of GB1 VFT[29]. Structures of isolated VFT and TM domains from other class C GPCR have been reported[30-32], in addition to more recently breakthrough that cryo-EM structures of full-length mGlu5 in apo state and in the presence of agonist have been determined both at overall 4 Å resolution, providing the first insights into the architecture of mGlu5 and structural framework of mGlu5 activation[33]. However, no structure of full-length $GABA_B$ receptor has been solved, limiting our understanding of the configuration of $GABA_B$ receptor. Moreover, molecular mechanism of class C GPCR signal transduction remains elusive, primarily owning to the lack of structural information of the receptor in various states, especially coupled to a down-streaming G protein. Here we present cryo-EM structures of human full-length heterodimeric $GABA_B$ receptor in the antagonist-bound inactive state and in the agonist/PAM-bound active state complexed with heterotrimeric G_{i1} protein, shedding lights on class C GPCR activation and providing a rational template for allosteric modulator design targeting dimeric interface of $GABA_B$ receptor.

Results

Cryo-EM structure determination of $GABA_B$ receptor

We first sought to obtain the heterodimeric human $GABA_B$ receptor in the fully inactive state, thus we overexpressed both GB1a and GB2 subunits in full length in mammalian cells and maintained 20 μM CGP54626, a potent antagonist with estimated nano-molar affinity to the receptor[34], through the sample preparation stage. The heterodimeric $GABA_B$ receptor was solubilized from the membrane using detergent. The following visualization by negative-staining EM displayed the existence of the intact heterodimer, and unlike detergent-

89 reconstituted mGlu5 in the inactive (apo) state with split micelles[33], $GABA_B$ receptor showed
90 one large disc-shaped micelle containing TMs from both subunits (Extended Data Fig. 1c, d).
91 Two-dimensional class averages of frozen specimen showed clear secondary structure features
92 for $GABA_B$ receptor dimer (Extended Data Fig. 2), confirming two TM bundles embedded in
93 the detergent micelle suggesting the more stable intersubunit interactions between TM domains
94 of $GABA_B$ receptor compared to that of mGlu5[33]. We therefore obtained cryo-EM images and
95 determined the density map for CGP54626-bound $GABA_B$ receptor using single particle cryo-
96 EM to an overall resolution of 3.0 Å. Local resolution calculations indicate a range of 2.4-3.4
97 Å in most map regions (Fig. 1a, Extended Data Fig. 2). The antagonist, VFT and TM domains
98 from both subunits are clearly visible in the cryo-EM map (Fig. 1a), except the sushi domains
99 at GB1 N terminus and coiled-coil domain at the $GABA_B$ receptor cytoplasmic tail, indicating
100 the dynamic nature of these two regions.

101 To prepare the stable and sufficient activated $GABA_B$–G_{i1} complex for cryo-EM study,
102 initial efforts were made to accomplish the complex formation under the condition in which the
103 receptor and the purified G_{i1} protein were incubated with baclofen, a commercially available
104 PAM BHFF in racemate form (rac-BHFF)[35] and G_i-binding protein scFv16[36], unfortunately
105 leading to the oligomerization of the receptor (data not shown). Considering the flexibility of
106 the coiled-coil domain indicated by the inactive structure of the full-length receptor, we thus
107 removed it and pull-down assay suggested that the receptor lacking of the coiled-coil domain
108 ($GABA_B$Δcc) exhibited increased expression level and improved complex formation yield of
109 $GABA_B$–G_{i1} (Extended Data Fig. 1e). These modifications do not alter receptor pharmacology
110 (hereafter referring $GABA_B$Δcc as $GABA_B$ unless noted otherwise) (Extended Data Fig. 1f).
111 We therefore formed the complex between the $GABA_B$ in mammalian cells, heterotrimeric G_{i1}
112 protein in insect cells before solubilization of the baclofen/PAM–$GABA_B$–G_{i1} complex using
113 lauryl maltoseneopentyl glycol and purification by tandem affinity and size-exclusion
114 chromatography (Extended Data Fig. 1g). Sample evaluation by negative-stain EM confirmed
115 the presence of G_{i1} protein and monodispersed particle distribution (Extended Data Fig. 1h). In
116 addition, cryo-EM analysis suggested multiply conformations spontaneously present in the
117 $GABA_B$–G_{i1} complex and three-dimensional classification revealed three major conformers,

118 with one of which representing G_{i1} protein engaged with GB1 and two of which representing
119 G_{i1} protein coupled to GB2 in distinct orientations (termed B1, B2a and B2b state, respectively).
120 We further refined these three conformers independently and obtained the reconstructions with
121 nominal resolutions of 8.8 Å, 6.8 Å and 8.6 Å, respectively, which were adequate for rigid-
122 body docking of the receptor and Gi1 independently to generate models for their relative
123 arrangement (Extended Data Fig. 3). Close visualization and superimposition of three
124 conformers with each other revealed no distinguishable difference in the receptor part, enabling
125 us to obtain high-resolution reconstruction for the active receptor (Extended Data Fig. 3, 4).
126 Therefore, we focused particle projection alignment on the VFT module and TM domain of the
127 receptor separately to improve the map quality and managed to obtain the maps with the
128 resolutions of 2.9 Å and 3.3 Å, respectively, which were subsequently combined to produce a
129 composite map for model building and refinement (Fig. 1b, Extended Data Fig. 3).

130 Taken together, the high-quality density maps allow the unambiguously placement of
131 antagonist (CGP54626), agonist (baclofen), PAM (BHFF) and most side chains of receptor
132 amino acids in both inactive and active states including all the extracellular loops (ECLs) and
133 intracellular loops (ICLs) with the exception of ICL2 (Fig. 3e, Extended Data Fig. 5, 7). Thus,
134 our structures provide accurate models of the full-length $GABA_B$ receptor in the inactive and
135 active states, shed lights on intersubunit interactions between GB1 and GB2, ligand recognition
136 and proposed models of G_{i1} engagement to the receptor. We also observed multiply ordered
137 cholesterols not only surrounding the periphery of both TM domains like many other
138 GPCRs[37,38], but also between two subunits primarily in the inactive state (Extended Data Fig.
139 6a). Surprisingly, well-defined density with the shape of phospholipid in the TM bundle of each
140 subunit was also observed in both states (Extended Data Fig. 6b-e). Considering the extensive
141 interactions between each phospholipid and the corresponding subunit and the consistent
142 presence of the phospholipids in both states, we speculated that phospholipids in the core
143 pockets are more likely structural components rather than allosteric modulators.

144

145 **Overall structure of $GABA_B$ receptor in the inactive state**

146 The overall architecture of $GABA_B$ receptor reveals that heterodimeric GB1 and GB2
147 subunits face each other side-by-side with a pseudo C2-symmetry. The linker between
148 extracellular VFT and TM domains within each subunit stands almost vertically to the bilayer.
149 The extended ECL2 β-hairpin interacts extensively with the linker through three-stranded anti-
150 parallel β-sheet, thus bridging VFT and TM domains in each subunit as a stalk (Fig. 1, 2a). This
151 arrangement is similar to mGlu5 receptor[33], yet lacking of cysteine-rich domain leading to the
152 shorten height of the receptor and partially contributing to the enhanced stability of the receptor
153 in the inactive conformation initially observed by negative stain EM (Extended Data Fig. 1d).
154 The structure of the $GABA_B$ VFT domains in the context of full-length receptor is very similar
155 to that of the corresponding crystal structures of soluble VFT in both inactive and active states
156 previously reported[29], with root mean squared deviation (r.m.s.d.) of 0.8 Å and 1.2 Å,
157 respectively (Extended Data Fig. 7a, b).

158 CGP54626 anchors at the lobe1 of GB1 VFT by largely hydrogen bonds and maintain the
159 receptor in the inactive state (Extended Data Fig. 7d). Accordingly, both VFT modules in the
160 structure of the antagonist-bound receptor are in an open state, resulting in the heterodimer
161 interfaces of $GABA_B$ in the VFT region mainly through two lobe1s with the buried surface area
162 of 702 $Å^2$ (Extended Data Fig. 8a). In addition, the interfaces in the inactive state also involve
163 the TM domains. Backbone separation distance of $GABA_B$ between the TM5 helices are 8 Å
164 in contrast to 17 Å of the inactive structure of mGlu5 (Extended Data Fig. 9a, b) and thus make
165 extensive contacts via lipid-mediate Van der Waals interactions at the extracellular half and salt
166 bridging at intracellular half (Fig. 3a-c). Salt bridge network close to the cytoplasmic membrane
167 surface is mediated by a charged-residue quartet from the TM3 and TM5 helices, namely
168 $H689^{3.55}$ and $E790^{5.60}$ of GB1, $H579^{3.55}$ and $E677^{5.60}$ of GB2 (superscript refers to the GPCRdb
169 numbering scheme)[39]. Moreover, we observed well-resolved and ordered densities along the
170 TM interface and assigned as putative cholesterols which connect a triplet of phenylalanine
171 residues packing against one another in the proximal to the polar network (GB1a: $F786^{5.56}$; GB2:
172 $F670^{5.53}$ and $F673^{5.56}$) and a quintuplet of leucine residues in the middle of TM region (GB1a:
173 $L779^{5.49}$, $L782^{5.52}$, $L783^{5.53}$; GB2: $L666^{5.49}$, $L669^{5.52}$), all of which are from TM5 helices (Fig.
174 3b). At the extracellular half of the TM interface, TM5 helices facing each other with short

175 uncharged sidechains form a deep crevice occupied by three putative cholesterols contributing
176 to an additional buried surface area of 419 $Å^2$, further substantially stabilizing the receptor in
177 the inactive conformation (Fig. 3a, Extended Data Fig. 6a). This novel TM interface represents
178 the structural signature of $GABA_B$ heterodimer TM domains in the inactive conformation.

179

180 **Conformational transition of $GABA_B$ heterodimer during activation**

181 Our 2.9 Å cryo-EM structure of the $GABA_B$ receptor in the active state reveals distinct
182 structural configuration in both VFT and TM domains to that in the inactive state (Fig. 2a).
183 Agonist baclofen anchors between two lobes of the GB1 VFT (Extended Data Fig. 7f) and
184 induces the closure of the GB1 VFT, with the lobe 2 of GB1 VFT undergoing a twist motion
185 and contacting the opposite lobe2 shortening the distance between the C termini of the two VFT
186 from 43 Å to 26 Å, in comparison to the distance changing from 45 Å to 32 Å as observed in
187 the previous structural studies of the soluble VFT (Extended Data Fig. 7a, b). This
188 conformational changes triggered by agonist binding propagates through the stalks and finally
189 relays to the TM domains, leading to translations of the GB1 and GB2 TMs by 31 Å and 19 Å,
190 respectively. Consequently, these structural transformations result in a TM6/TM6 interface (Fig.
191 2b, Fig. 3d), consistent with previous cross-linking studies[40]. This interface is also observed in
192 the agonist-bound structure of the mGlu5 homodimer[33], suggesting the TM6/TM6 interface is
193 likely a hallmark of activation of class C GPCR.

194 Akin to the TM interface in the inactive $GABA_B$ receptor, the interactions between the
195 TM6/TM6 helices are strengthened by the hydrophobic and hydrophilic contacts. Compared to
196 the lipid-mediated hydrophobic interactions at the extracellular half in the inactive state, the
197 two TM6 helices in the active conformation directly pack together at their extracellular half via
198 hydrophobic interactions, involving $V814^{6.48}$, $I818^{6.52}$, $V822^{6.56}$, $I825^{6.59}$, $L826^{ECL3}$, $A832^{7.27}$,
199 $F836^{7.31}$ from GB1 and $M694^{6.41}$, $I701^{6.48}$, $M702^{6.49}$, $I705^{6.52}$, $A789^{6.55}$, $V709^{6.56}$, $L712^{6.59}$,
200 $T713^{ECL3}$, $Q716^{ECL3}$, $V719^{7.27}$ from GB2 and contributing to a buried surface area of 507 $Å^2$
201 (Fig. 3d, Extended Data Fig. 8b). In the middle of the TM interface is a hydrogen bond network
202 locked by the $Y^{6.44}$ and $N^{6.45}$ from both subunits, which are conserved through class C GPCR

203 family (Fig. 3d, Extended Data Table 1). The TM6/TM6 interface is further stabilized by BHFF,
204 a potent and selective $GABA_B$ receptor PAM agonist (PAM-ago), which can enhance the
205 potency of endogenous agonist GABA and also directly active $GABA_B$ receptor in the absence
206 of other agonists with the mechanism of act unknown[41]. The high-resolution cryo-EM map
207 enables us identify and unambiguously assign the BHFF into the density located in the cavity
208 formed by the intracellular tips of TM5-TM6 of GB1 and TM6 of GB2 (Fig. 3e, f). It's
209 noteworthy that we found the pure enantiomer (+)-BHFF fitting into the density better than (–)-
210 BHFF, in agreement with previous pharmacological studies which suggested that rac- and (+)-
211 BHFF could enhance the GABA potency by 15.3-fold and 87.3-fold, respectively. The (+)-
212 BHFF is mainly recognized by the hydrophobic interactions, including $A788^{5.58}$, $Y789^{5.59}$,
213 $M807^{6.41}$, $Y810^{6.44}$ of GB1 and $K690^{6.37}$, $Y691^{6.38}$, $M694^{6.41}$ of GB2. Additionally, 3-hydroxy
214 group and ketone are hydrogen-bonded to $K792^{ICL3}$ of GB1(Fig. 3f). Given that BHFF can
215 directly activate the $GABA_B$ receptor and both its potency and efficacy could be enhanced in
216 the presence of GABA, we anticipate that the cavity where BHFF occupied might be
217 allosterically modulated by the orthosteric binding pocket and *vice versa*. We thus identified a
218 novel PAM-binding pocket within a GPCR dimer and thus provide a template for future
219 structure-based drug design of allosteric modulators targeting class C GPCR dimerization
220 interface.

221

222 **Structure and activation of TM domain of $GABA_B$ receptor**

223 All the available TM structures of class C GPCRs are in the apo or inactive conformation
224 including cryo-EM structure of the full-length mGlu5 bound to agonist[33]. Superposition of
225 individual TM domains between $GABA_B$ and other class C GPCRs including mGlu1 and
226 mGlu5 reveals distinct structural features for TM5, TM7, ECL1, ECL2 and ICL3 (Extended
227 Data Fig. 9c). Extracellular tips of TM5 and TM7 helices of $GABA_B$ receptor demonstrate
228 obvious outward shifting by 5 Å, likely resulting from the presence of endogenous phospholipid
229 in the center of TM bundle which extensively contacts TM3, 5, 6 and 7 (Extended Data Fig.
230 6a). ECL2 of $GABA_B$ spanning in a β-hairpin configuration is 5-residue extended relative to
231 other class C GPCRs, leading to more tight interaction with the linker and enabling the direct

232 contacts with the bottom of VFT (Fig. 4, Extended Data Fig. 9c). Therefore, this extension
233 facilitates the conformational changes of VFT induced by agonist binding conducting to TM
234 domain. Moving to the intracellular loops, the most profound difference is the position of ICL3,
235 which is proposed to play a crucial role in G-protein coupling[25]. The ICL3 of $GABA_B$ receptor
236 is comprised of 11 residues for both subunits (residues 791-801 for GB1 and residues 678-688
237 for GB2) and stretched over the TM pocket at the cytoplasmic surface. The conformation of
238 ICL3 is stabilized by the polar network formed by $S515^{12.53}$, $N520^{2.39}$, $K574^{3.50}$, $N687^{6.34}$ and
239 $D688^{6.35}$ which are highly conserved among class C GPCRs and further strengthened by
240 hydrophobic interactions between $L511^{12.49}$, $M514^{12.52}$, $A675^{5.58}$, $W676^{5.59}$ (Extended Data Fig.
241 10a-c). We anticipate that the unique conformation of ICL3 in $GABA_B$ receptor restricts the
242 access of G proteins or β-arrestins to the receptor similar to the role of helix 8 of the angiotensin
243 II receptor AT_2R[42]. In contrast, the same loop from mGlu1 and mGlu5 is 2-residue shorter and
244 stands almost perpendicular to the bilayer, leaving the TM cavity at the cytoplasmic side more
245 accessible to the effector proteins (Extended Data Fig. 9c).

246 The overall structures of the $GABA_B$ TM domains are highly similar in the inactive state
247 with r.m.s.d. of 0.939 Å as expected, considering that the two TM domains share 72% sequence
248 homology. Although upon activation the apical tip of GB1 ECL2 shifts 6 Å measured at Cα
249 atom of $I750^{ECL2}$ residue, the extracellular conformational changes induced by agonist binding
250 do not relay to GB1 TM domain through the stalk, which is mostly unchanged (r.m.s.d. of
251 2.23Å) (Fig. 4a). In contrast, substantial conformational changes occur at GB2 stalk region
252 (r.m.s.d. of 3.94 Å) translating by 5.6 Å measured at I469, triggering the extracellular tips of
253 TM4 and TM5 shifting 2.0 Å and 2.9 Å to the opposite direction measured at $D619^{4.54}$ and
254 $T654^{5.37}$, respectively (Fig. 4b). Consequently, the intracellular tip of GB2 TM3 undergoes 5.2
255 Å shifting (measured at Cα atom of $I581^{3.57}$) towards TM4 and TM2, leading to a 2.7 Å and 1.7
256 Å outward movement measured at Cα atom of $L598^{4.33}$ and at Cα atom of $M519^{2.38}$,
257 respectively. The most profound conformational changes at the cytoplasmic half locate at TM5-
258 ICL3. GB2 TM5 extends one helical turn and shifts 5.4 Å measured at Cα atom of $W678^{5.61}$
259 toward TM3, resulting in the breaking of the ionic interactions between $N687^{6.34}$, $D688^{6.35}$and
260 $S515^{12.53}$, $N520^{2.39}$, $K574^{3.50}$, and thus the ICL3 stands up uncovering the lid of TM pocket at

261 the cytoplasmic side (Extended Data Fig. 10b). Taken together, the orchestration of the
262 conformational changes in the TM domain of GB2 subunit enables it accommodating the down-
263 streaming Gi/o protein to initiate the intracellular signaling.

264

265 **Gi heterogeneously coupling to $GABA_B$ receptor heterodimer**

266 The structural rearrangement of GB2 TM domain barely exposes residues from TM helices
267 and thus creates a shallow binding site for the heterotrimeric G_{i1} protein (Fig. 5a-c), whereas
268 all the available GPCR–G structures show a deep cavity formed by the outward movement of
269 the cytoplasmic half of TM6 together with TM2, 3, 5, and 7[43]. This remarkable shallow pocket
270 disallows the insertion of the α5-helix of the Gαi Ras-like domain into the receptor TM domain
271 and is probably responsible for the conformational heterogeneity present in the $GABA_B$–G_{i1}
272 complex. We identified three thermostable conformations demonstrating well-resolved density
273 for G_{i1} protein, which are B2a, B2b and B1 states with the population distribution of 74%, 9%
274 and 17% among the sub dataset, respectively (Fig. 5a-c, Extended Data Fig. 3), this observation
275 suggests that G_{i1} protein predominantly couples to GB2 subunit which is consistent with the
276 asymmetric activation model of $GABA_B$ receptor. Superposing the isolated GB1–G_i structure
277 from B1 state to the heterodimer structure of either B2a or B2b state shows the potential steric
278 hindrance between the two Ras-like domains of G_{i1}, perfectly explaining why only one G
279 protein binds to the $GABA_B$ receptor at a time (Fig. 5d).

280 The interface between the activated $GABA_B$ receptor and G_{i1} protein in B2a state involves
281 ICLs and intracellular tip of TM3 of the receptor and α5-helix of the Gαi Ras-like domain,
282 primarily stabilized by hydrophobic interactions and complementary change interactions (Fig.
283 5a, Extended Data Fig. 10d). The carboxyl terminal α5-helix of the $G\alpha_i$ overlaps the position
284 of GB2 ICL3 in the inactive state, explaining the requirement for GB2 ICL3 opening to
285 accommodate the $G_{i/o}$ protein. Previous studies showed that the single mutation L686P in the
286 ICL3 of GB2 suppresses the activation of G protein in either HEK293 cells or cultured neurons,
287 highlighting the critical role of ICL3 of GB2 for the coupling of the heterodimeric $GABA_B$
288 receptor to G-proteins[25], in agreement with our structural findings. Consistently, the α5-helix is

289 also the sole coupling site with the receptor in the other two states (Fig. 5b, c, Extended Data
290 Fig. 10e, f). Interestingly, the α5-helix of the Gαi in three $GABA_B$–G_{i1} states translates
291 downwards to the similar extent (about 10 Å) relative to that of class A GPCR–G_i complex in
292 the canonical and noncanonical states (Fig. 5e), leading to the absence of Gβγ in the receptor–
293 G_{i1} interface. However, G_{i1} in B2b and B1 states is rotated by about ~90° to opposite side of
294 that in B2a state relative to the receptor, positioning G_{i1} in the complex in distinct arrangement
295 (Fig. 5f). Surprisingly, unlike class A and B GPCRs, TM6 holds its position in response to
296 activation, constrained by the TM6/TM6 interface in the active state (Fig. 5g).

297 Intriguingly, the observation of the $GABA_B$–G_{i1} complex in GB1 state provides the
298 structural explanation of the basal activity of $GABA_B$ receptor given that GB1 TM domain
299 shares the same conformation in the inactive and active states, in agreement with that expression
300 of GB1 alone at the cell surface activates ERK1/2 through $G_{i/o}$-dependent pathway[27,28].
301 Considering the significant difference at population between the two B2 states, we anticipate
302 that B2a is likely more thermodynamically stable and therefore forms after the B2b state along
303 the activation pathway of G protein. Similar phenomenon was observed in the neurotensin
304 receptor 1(NTSR1)–G_{i1} complex[44].

305

306 **Conclusion**

307 $GABA_B$ receptor represents the first example of an obligatory GPCR heterodimer,
308 functions as an allosteric multi-domain protein and oscillates between the inactive and active
309 states[21]. Ligands or G proteins interplay with the pre-existing states of the receptor based on
310 "selection mode of allostery"[21,45]. In this study, by synchronizing receptor in the inactive state
311 with the presence of antagonist or completely stabilizing receptor in the active state with the
312 presence of agonist, PAM and G_{i1} protein, we determined the atomic-resolution cryo-EM
313 structures of a human full-length $GABA_B$ heterodimer in both inactive and active states. The
314 high-resolution cryo-EM maps not only confirmed the binding mode of CGP54626 and
315 baclofen observed in the crystal structures of $GABA_B$ VFT[29], but also revealed the working
316 mechanism of BHFF as PAM agonist, which stabilizes a novel intersubunit interface in the TM

317 domains of the active $GABA_B$ receptor. Surprisingly, endogenous phospholipids settle inside
318 each TM extracellular pore, equivalent to classical orthosteric binding pocket for class A GPCR,
319 in all $GABA_B$ structures obtained in this work and lead to a distinct conformational
320 configuration of $GABA_B$ TM domains compared to other class C GPCRs, suggesting the
321 presence of these lipids may function as structural components which is probably a unique
322 phenomenon to $GABA_B$ receptor.

323 Structural comparison of $GABA_B$ receptor in different states enabled us to propose a
324 structural rearrangement for $GABA_B$ receptor activation. Agonist binding induces the
325 compaction of two VFTs (Fig. 2, Extended Data Fig. 7a, b), propagating through the stalk
326 domains to the TM domains, which in turn reorients the TM interface between two subunits
327 from TM3-TM5/TM3-TM5 in the inactive state to TM6/TM6 in the active state, in perfect
328 agreement with previous crosslinking data for $GABA_B$ receptor and mGlu homodimers[40,46].
329 Therefore, the overall domain rearrangements upon activation of $GABA_B$ receptor resemble the
330 published cryo-EM structures of mGlu5[33], suggesting this reorientation of TM domains is
331 possibly the hallmark of class C GPCR activation.

332 We determined cryo-EM structures of a GPCR heterodimer in a complex with G_{i1} protein,
333 which only can couple to either one of the subunit at one time to avoid steric hindrance by the
334 presence of Ras-like domain of two Gα proteins. The unprecedented structures reveal novel
335 conformational changes within the GB2 TM domain to accommodate the G_i protein involving
336 the opening of ICL3 and movement of TM3, 4 and 5 helices, enabling $GABA_B$ receptor
337 predominantly couples to G_{i1} protein through GB2 subunit. However, the structure of $GABA_B$–
338 G_{i1} complex coupling via GB1 demonstrates that GB1 couples to G_i protein at certain
339 circumstance. Indeed, GB1 in C. elegans directly couples to $G_{i/o}$ protein-dependent
340 signaling[47,48], indicating that GB1 retains the capacity for Gi protein coupling during evolution.
341 Common activation mechanism for G protein activation by GPCRs has been proposed, in which
342 the landmark of GPCR activation is the outwards movement of TM6 forming a cavity to
343 accommodate the G proteins or β-arrestins, reflecting the convergence of activation pathways
344 in class A, B and F GPCRs[43,49,50]. However, the $GABA_B$–G_{i1} engagement patterns have not been
345 observed in the structures of other GPCR-G complexes, implying the complex of GPCR-G

complex, especially for GPCR in dimeric form. Further studies are required to determine the high-resolution structure of $GABA_B$–G_{i1} complex to decipher the molecular mechanism of $GABA_B$–G protein assembly. Additional structural studies are also needed to determine whether similar G protein engagement are present in other class C GPCRs.

Acknowledgements

We thank S. Chang for technical support in cryo-EM data collection at the Center of Cryo-Electron Microscopy, Zhejiang University; C. Ma for support in protein purification at the Protein Facilities, Zhejiang University School of Medicine. J.L. was supported by the Ministry of Science and Technology (2018YFA0507003), the National Natural Science Foundation of China (NSFC) (81720108031, 81872945, 31721002 and 31420103909), the Program for Introducing Talents of Discipline to the Universities of the Ministry of Education (B08029), and the Mérieux Research Grants Program of the Institut Mérieux. Y.Z. was supported by the National Science Foundation of China (81922071) and the National Key Basic Research Program of China (2019YFA0508800).

Author contributions

C.S. designed the constructs, expressed and purified the antagonist-bound $GABA_B$ and the agonist/PAM stimulated $GABA_B$-G_{i1} complex for cryo-EM data collection with the help of S.Z.; C.S., R.Z. and C.L. performed pull-down assay; C.L. and L.-N.C. expressed and purified scFv16; C.X. performed BRET assay; D.-D.S. evaluated the sample by negative-stain EM; C.M. prepared the cryo-EM grids; C.M., D.-D.S. collected the cryo-EM data; C.M. performed cryo-EM map calculation, model building and structure refinement; C.M. and C.S. analyzed the structures and prepared the figures with the help of D.-D.S., Q.S. and Z.J.; Y.Z. and J.L. conceived and supervised the project, analyzed the structures, and wrote the manuscript with input from all the authors.

COMPETING INTERESTS: The authors declare no competing interests.

References

1 Barnard, E. A. *et al.* International Union of Pharmacology. XV. Subtypes of gamma-aminobutyric acidA receptors: classification on the basis of subunit structure and receptor function. *Pharmacol Rev* **50**, 291-313 (1998).

2 Bettler, B. & Tiao, J. Y. Molecular diversity, trafficking and subcellular localization of GABAB receptors. *Pharmacology & therapeutics* **110**, 533-543, doi:10.1016/j.pharmthera.2006.03.006 (2006).

3 Kaupmann, K. *et al.* GABA(B)-receptor subtypes assemble into functional heteromeric complexes. *Nature* **396**, 683-687, doi:10.1038/25360 (1998).

4 Mott, D. D. & Lewis, D. V. The pharmacology and function of central GABAB receptors. *International review of neurobiology* **36**, 97-223, doi:10.1016/s0074-7742(08)60304-9 (1994).

5 Bettler, B., Kaupmann, K., Mosbacher, J. & Gassmann, M. Molecular structure and physiological functions of GABA(B) receptors. *Physiological reviews* **84**, 835-867, doi:10.1152/physrev.00036.2003 (2004).

6 Luscher, C., Jan, L. Y., Stoffel, M., Malenka, R. C. & Nicoll, R. A. G protein-coupled inwardly rectifying K+ channels (GIRKs) mediate postsynaptic but not presynaptic transmitter actions in hippocampal neurons. *Neuron* **19**, 687-695, doi:10.1016/s0896-6273(00)80381-5 (1997).

7 Tu, H. *et al.* GABAB receptor activation protects neurons from apoptosis via IGF-1 receptor transactivation. *The Journal of neuroscience : the official journal of the Society for Neuroscience* **30**, 749-759, doi:10.1523/jneurosci.2343-09.2010 (2010).

8 Lin, X. *et al.* An activity-based probe reveals dynamic protein-protein interactions mediating IGF-1R transactivation by the GABA(B) receptor. *Biochem J* **443**, 627-634, doi:10.1042/bj20120188 (2012).

9 Samanta, D. & Zarate, Y. A. Widening phenotypic spectrum of GABBR2 mutation. *Acta neurologica Belgica* **119**, 493-496, doi:10.1007/s13760-019-01088-5 (2019).

10 Dalmau, J. & Graus, F. Antibody-Mediated Encephalitis. *N Engl J Med* **378**, 840-851, doi:10.1056/NEJMra1708712 (2018).

11 Hoftberger, R. *et al.* Encephalitis and GABAB receptor antibodies: novel findings in a new case series of 20 patients. *Neurology* **81**, 1500-1506, doi:10.1212/WNL.0b013e3182a9585f (2013).

12 Froestl, W. Chemistry and pharmacology of GABAB receptor ligands. *Advances in pharmacology (San Diego, Calif.)* **58**, 19-62, doi:10.1016/s1054-3589(10)58002-5 (2010).

13 Addolorato, G. *et al.* Baclofen efficacy in reducing alcohol craving and intake: a preliminary double-blind randomized controlled study. *Alcohol and alcoholism (Oxford, Oxfordshire)* **37**, 504-508, doi:10.1093/alcalc/37.5.504 (2002).

14 Chang, E. *et al.* A Review of Spasticity Treatments: Pharmacological and Interventional Approaches. *Crit Rev Phys Rehabil Med* **25**, 11-22, doi:10.1615/CritRevPhysRehabilMed.2013007945 (2013).

15 Xu, X. M., Wei, Y. D., Liu, Y. & Li, Z. X. Gamma-hydroxybutyrate (GHB) for

418 narcolepsy in adults: an updated systematic review and meta-analysis. *Sleep medicine*
419 **64**, 62-70, doi:10.1016/j.sleep.2019.06.017 (2019).
420 16 Kniazeff, J., Prezeau, L., Rondard, P., Pin, J. P. & Goudet, C. Dimers and beyond: The
421 functional puzzles of class C GPCRs. *Pharmacology & therapeutics* **130**, 9-25,
422 doi:10.1016/j.pharmthera.2011.01.006 (2011).
423 17 Romano, C., Yang, W. L. & O'Malley, K. L. Metabotropic glutamate receptor 5 is a
424 disulfide-linked dimer. *The Journal of biological chemistry* **271**, 28612-28616,
425 doi:10.1074/jbc.271.45.28612 (1996).
426 18 Bai, M., Trivedi, S. & Brown, E. M. Dimerization of the extracellular calcium-sensing
427 receptor (CaR) on the cell surface of CaR-transfected HEK293 cells. *The Journal of*
428 *biological chemistry* **273**, 23605-23610, doi:10.1074/jbc.273.36.23605 (1998).
429 19 White, J. H. *et al.* Heterodimerization is required for the formation of a functional
430 GABA(B) receptor. *Nature* **396**, 679-682, doi:10.1038/25354 (1998).
431 20 Kuner, R. *et al.* Role of heteromer formation in GABAB receptor function. *Science*
432 *(New York, N.Y.)* **283**, 74-77, doi:10.1126/science.283.5398.74 (1999).
433 21 Pin, J. P. & Bettler, B. Organization and functions of mGlu and GABAB receptor
434 complexes. *Nature* **540**, 60-68, doi:10.1038/nature20566 (2016).
435 22 Pagano, A. *et al.* C-terminal interaction is essential for surface trafficking but not for
436 heteromeric assembly of GABA(b) receptors. *The Journal of neuroscience : the official*
437 *journal of the Society for Neuroscience* **21**, 1189-1202 (2001).
438 23 Ng, G. Y. *et al.* Identification of a GABAB receptor subunit, gb2, required for
439 functional GABAB receptor activity. *The Journal of biological chemistry* **274**, 7607-
440 7610, doi:10.1074/jbc.274.12.7607 (1999).
441 24 Malitschek, B. *et al.* The N-terminal domain of gamma-aminobutyric Acid(B)
442 receptors is sufficient to specify agonist and antagonist binding. *Mol Pharmacol* **56**,
443 448-454, doi:10.1124/mol.56.2.448 (1999).
444 25 Duthey, B. *et al.* A single subunit (GB2) is required for G-protein activation by the
445 heterodimeric GABA(B) receptor. *The Journal of biological chemistry* **277**, 3236-3241,
446 doi:10.1074/jbc.M108900200 (2002).
447 26 Robbins, M. J. *et al.* GABA(B2) is essential for g-protein coupling of the GABA(B)
448 receptor heterodimer. *J Neurosci* **21**, 8043-8052 (2001).
449 27 Richer, M. *et al.* GABA-B(1) receptors are coupled to the ERK1/2 MAP kinase
450 pathway in the absence of GABA-B(2) subunits. *Journal of molecular neuroscience :*
451 *MN* **38**, 67-79, doi:10.1007/s12031-008-9163-6 (2009).
452 28 Baloucoune, G. A. *et al.* GABAB receptor subunit GB1 at the cell surface
453 independently activates ERK1/2 through IGF-1R transactivation. *PLoS One* **7**, e39698,
454 doi:10.1371/journal.pone.0039698 (2012).
455 29 Geng, Y., Bush, M., Mosyak, L., Wang, F. & Fan, Q. R. Structural mechanism of ligand
456 activation in human GABA(B) receptor. *Nature* **504**, 254-259,
457 doi:10.1038/nature12725 (2013).
458 30 Muto, T., Tsuchiya, D., Morikawa, K. & Jingami, H. Structures of the extracellular
459 regions of the group II/III metabotropic glutamate receptors. *Proceedings of the*
460 *National Academy of Sciences of the United States of America* **104**, 3759-3764,
461 doi:10.1073/pnas.0611577104 (2007).

31 Wu, H. *et al.* Structure of a class C GPCR metabotropic glutamate receptor 1 bound to an allosteric modulator. *Science (New York, N.Y.)* **344**, 58-64, doi:10.1126/science.1249489 (2014).

32 Dore, A. S. *et al.* Structure of class C GPCR metabotropic glutamate receptor 5 transmembrane domain. *Nature* **511**, 557-562, doi:10.1038/nature13396 (2014).

33 Koehl, A. *et al.* Structural insights into the activation of metabotropic glutamate receptors. *Nature* **566**, 79-84, doi:10.1038/s41586-019-0881-4 (2019).

34 Jones, K. A. *et al.* GABA(B) receptors function as a heteromeric assembly of the subunits GABA(B)R1 and GABA(B)R2. *Nature* **396**, 674-679, doi:10.1038/25348 (1998).

35 Malherbe, P. *et al.* Characterization of (R,S)-5,7-di-tert-butyl-3-hydroxy-3-trifluoromethyl-3H-benzofuran-2-one as a positive allosteric modulator of GABAB receptors. *British journal of pharmacology* **154**, 797-811, doi:10.1038/bjp.2008.135 (2008).

36 Koehl, A. *et al.* Structure of the micro-opioid receptor-Gi protein complex. *Nature* **558**, 547-552, doi:10.1038/s41586-018-0219-7 (2018).

37 Zhao, L. H. *et al.* Structure and dynamics of the active human parathyroid hormone receptor-1. *Science (New York, N.Y.)* **364**, 148-153, doi:10.1126/science.aav7942 (2019).

38 Ma, S. *et al.* Molecular Basis for Hormone Recognition and Activation of Corticotropin-Releasing Factor Receptors. *Molecular cell* **77**, 669-680.e664, doi:10.1016/j.molcel.2020.01.013 (2020).

39 van der Kant, R. & Vriend, G. Alpha-bulges in G protein-coupled receptors. *International journal of molecular sciences* **15**, 7841-7864, doi:10.3390/ijms15057841 (2014).

40 Xue, L. *et al.* Rearrangement of the transmembrane domain interfaces associated with the activation of a GPCR hetero-oligomer. *Nat Commun* **10**, 2765, doi:10.1038/s41467-019-10834-5 (2019).

41 Koek, W., Cheng, K. & Rice, K. C. Discriminative stimulus effects of the GABAB receptor-positive modulator rac-BHFF: comparison with GABAB receptor agonists and drugs of abuse. *The Journal of pharmacology and experimental therapeutics* **344**, 553-560, doi:10.1124/jpet.112.202226 (2013).

42 Zhang, H. *et al.* Structural basis for selectivity and diversity in angiotensin II receptors. *Nature* **544**, 327-332, doi:10.1038/nature22035 (2017).

43 Glukhova, A. *et al.* Rules of Engagement: GPCRs and G Proteins. *ACS pharmacology & translational science* **1**, 73-83, doi:10.1021/acsptsci.8b00026 (2018).

44 Kato, H. E. *et al.* Conformational transitions of a neurotensin receptor 1-Gi1 complex. *Nature* **572**, 80-85, doi:10.1038/s41586-019-1337-6 (2019).

45 Xu, C., Zhang, W., Rondard, P., Pin, J. P. & Liu, J. Complex GABAB receptor complexes: how to generate multiple functionally distinct units from a single receptor. *Front Pharmacol* **5**, 12, doi:10.3389/fphar.2014.00012 (2014).

46 Xue, L. *et al.* Major ligand-induced rearrangement of the heptahelical domain interface in a GPCR dimer. *Nature chemical biology* **11**, 134-140, doi:10.1038/nchembio.1711 (2015).

506 47 Yuan, F. *et al.* GABA receptors differentially regulate life span and health span in C.
507 elegans through distinct downstream mechanisms. *Am J Physiol Cell Physiol* **317**,
508 C953-C963, doi:10.1152/ajpcell.00072.2019 (2019).
509 48 Chun, L. *et al.* Metabotropic GABA signalling modulates longevity in C. elegans.
510 *Nature communications* **6**, 8828, doi:10.1038/ncomms9828 (2015).
511 49 Qi, X. *et al.* Cryo-EM structure of oxysterol-bound human Smoothened coupled to a
512 heterotrimeric Gi. *Nature* **571**, 279-283, doi:10.1038/s41586-019-1286-0 (2019).
513 50 Krumm, B. & Roth, B. L. A Structural Understanding of Class B GPCR Selectivity
514 and Activation Revealed. Structure (London, England : 1993) 28, 277-279,
515 doi:10.1016 /j.str.2020.02.004 (2020).

516 ## Methods

517 ### Constructs

518 Human $GABA_B$ receptor with the HA signal peptide including GB1a (UniProt: Q9UBS5) and
519 GB2 (UniProt: O75899) were cloned into pEG BacMam vector, respectively[51]. To facilitate
520 expression and purification, an 8× histidine tag and 3C protease cleavage site were inserted at
521 the C-terminus of GB1a subunit, while a Flag epitope tag (DYKDDDD) and a 2×GSG linker
522 were added to the N-terminus of GB2 subunit. Both GB1 and GB2 with a long, flexible C
523 terminal affected the level of expression. Therefore, we utilized different constructs with
524 cleavable C-terminal domains: GB1 and GB2 were truncated after coiled-coil domain; GB1△cc
525 and GB2△cc were truncated before coiled-coil domain; GB1△C means the C-terminus of GB1
526 was removed. In addition, we construct the Dual pEG BacMam vector could express GB1 and
527 GB2 by combining two plasmids using homologous recombinant enzyme to increase
528 expression level.

529

530 ### Expression and purification of inactive $GABA_B$ receptor

531 GB1a (GB1cc residues 15-919) and GB2 (GB2cc residues 42-819) were co-expression in
532 HEK293F cells. In brief, purified plasmid DNA was mixed with PEI 25K in a 3:1 ratio of PEI
533 to DNA (w/w) followed by addition to HEK293F cells when density reached around 2.8
534 million/ml[52]. 10 mM sodium butyrate was added after 16-18 hours post-infection, then cells
535 grown for 3 days at 30 °C before harvested[51,52]. The infected cells were collected by
536 centrifugation at 1000 g for 15 min and washed once with 1×PBS buffer. Cells were suspended
537 in 50 mM HEPES pH 7.5, 150 mM NaCl, 10% glycerol, 2 mM $MgCl_2$, 20 μM CGP54626
538 (Tocris Bioscience) with cocktail followed by homogenization. The membrane was solubilized
539 for 3 hours at 4 °C with 0.5% (w/v) lauryl maltose neopentyl glycol (LMNG, Anatrace), 0.1%
540 (w/v) cholesteryl hemisuccinate (CHS, Anatrace). After centrifugation at 30,000 g for 30 min,
541 the supernatant was bound to Ni-NTA column and further loaded onto M1 anti-FLAG affinity
542 resin. The protein was eluted in elution buffer consisting of 50 mM Hepes pH 7.5, 150 mM
543 NaCl, 0.01% LMNG, 0.002% CHS, 20 μM CGP54626, 5 mM EGTA and 0.1 mg/mL FLAG

544 peptide. The $GABA_B$ receptor was concentrated in a 100-kDa cutoff Vivaspin (Millipore) filter
545 and run on a Superose™ 6 Increase column (GE Healthcare).

546

547 **Expression of heterotrimeric Gi**

548 Heterotrimeric Gi was expressed as previously described[53]. In general, the dominant-negative
549 rat Gαi1 was introduced four mutations (S47N, G203A, E245A and A326S) and a 6× histidine
550 tag was added at the N-terminus of the β subunit. The Sf9 insect cells (Expression Systems) at
551 a density of 2.4 million/ml were infected with both Gαi and Gβγ virus in a 1:1 ratio. Cells were
552 harvested 48 hours after infection and collected by centrifugation at 1000g for 15 min. Finally,
553 the cells were washed once with 1×PBS buffer and snap frozen in liquid nitrogen for later use.

554

555 **Expression and purification of scFv16**

556 The secreted scFv16 was expressed and purified by using the bac-to-bac system as previously
557 described[36]. In brief, the virus of scFv16 with 6× histidine tag at the C-terminus was infected
558 in Trichoplusia ni Hi5 insect cells for 48 hours. The pH of Supernatant was balanced by addition
559 of Tris pH 8.0 while Chelating agents were removed by addition of 1 mM nickel chloride and
560 5 mM calcium chloride. After incubation with stirring at room temperature for 1 hour the
561 supernatant was loaded onto Ni-NTA resin and further eluted in elution buffer consisting of 20
562 mM Hepes pH 7.5, 500 mM NaCl, and 250 mM imidazole. The sample was first treated with
563 3C protease, then diluted and reloaded onto the Ni-NTA column to remove the 6×histidine tag.
564 The flow-through was collected and purified over gel filtration chromatography using a
565 Superdex 200 column. Finally, the concentrated of scFv16 was flash frozen in liquid nitrogen
566 until further use.

567

568 **Formation and purification of the $GABA_B$-G_i-scFv16 complex**

569 GB1a (GB1ΔC residues 15-860) and GB2 (GB2Δcc residues 42-780) were chosen to form
570 $GABA_B$-G_{i1} complex. The conditions for $GABA_B$ expression in HEK293F cells described

571 earlier. Purified plasmid DNA was mixed with PEI 25K in a 3:1 ratio of PEI to DNA (w/w) was
572 added to HEK293F when density reached around 2.8 million/ml. The infected HEK293F cells
573 and the expressed G_{i1} cells together were suspended and disrupted in 50mM HEPES pH 7.5,
574 150 mM NaCl, 10% glycerol, 2 mM $MgCl_2$, 100 μM baclofen and 50 μM BHFF (Tocris
575 Bioscience) with cocktail followed by addition of 50 mU/ml apyrase and 1.0 mg scFv16. The
576 membrane was solubilized with 0.5% (w/v) LMNG and 0.1% (w/v) CHS for 3 hours at 4 °C
577 and separated by centrifugation at 30,000g for 30 min. The supernatant was bound to Ni-NTA
578 column and further loaded onto M1 anti-FLAG affinity resin. The protein was eluted in elution
579 buffer consisting of 50 mM Hepes pH 7.5, 150 mM NaCl, 0.01% LMNG, 0.002% CHS, 100
580 μM baclofen and 50 μM BHFF, 5 mM EGTA and 0.1 mg/mL FLAG peptide. The $GABA_B$-Gi-
581 SCFV16 complex was concentrated in a 100-kDa cutoff Vivaspin (Millipore) filter and run on
582 a Superose™ 6 Increase column.

583

584 **G protein pull-down analysis**

585 Three different group truncations of $GABA_B$ receptor were cloned into pEG BacMam vector,
586 respectively. Flag epitope tag (DYKDDDD) and a 2×GSG linker were added to the N terminus
587 of GB2. Different group truncations of $GABA_B$ receptor were expression in 30 ml HEK293F
588 cells while Heterotrimeric Gi was expression in 30 ml Sf9 insect cells. These cells were
589 suspended in 50 mM HEPES pH 7.5, 150 mM NaCl, 10% glycerol, 2 mM $MgCl_2$, 100 μM
590 baclofen and 50 μM BHFF with cocktail followed by homogenization. 50 mU/ml apyrase and
591 0.03mg scFv16 were added to incubate 3 hours. The membrane was solubilized with 0.5% (w/v)
592 L-MNG and 0.1% (w/v) CHS for another 3 hours at 4 °C. After centrifugation, the supernatant
593 was incubated with 25μl M1 anti-FLAG affinity resin for 1 hour at 4 °C and then eluted in 50
594 μl elution buffer supplemented with 100 μM baclofen and 50 μM rac-BHFF, 5 mM EGTA and
595 0.1 mg/mL FLAG peptide. Sample collected from different truncations were analyzed by SDS-
596 PAGE.

597

598 **Bioluminescence resonance energy transfer (BRET) assay**

599 HEK293 cells were transfected with wild type or truncation (GB1ΔC-GB2Δcc) $GABA_B$
600 receptor, Gβ1, Venus-Gγ2 and Gαi-Rluc8 by lipofectamine 2000 and split into 96-well flat-
601 bottomed white microplates. After 24 h transfection, cells were washed and starved in PBS at
602 37 °C for 1 hour. BRET measurements were performed using the Mithras LB 940 (Berthold
603 Technologies, German). The signals emitted by the donor (460–500 nm band-pass filter, Em
604 480) and the acceptor entity (510–550 nm band-pass filter, Em 530) were recorded after the
605 addition of 5 μM Coelenterazine H. All measurements were performed at 37 °C. The BRET
606 signal was determined by calculating the ratio of the Em 530 and Em 480. The net BRET ratio
607 was defined as the experimental BRET signal values with the baseline subtracted (basal BRET
608 ratio), which was recorded before the stimulation of cells. For dose-response experiments, data
609 were analyzed using nonlinear curve fitting for the log (agonist) vs. Response (three parameters)
610 curves in GraphPad Prism software.

611

612 **Cryo-EM grid preparation and data collection**

613 For the preparation of Cryo-EM grids, 3 μl of the purified antagonist bound $GABA_B$
614 heterodimer or baclofen/BHFF bound–$GABA_B$–G_{i1} complex at ~2.0 mg/ml was applied onto a
615 glow-discharged 200 mesh holey carbon grid (Quantifoil R1.2/1.3). The grids were blotted and
616 then plunge-frozen in liquid ethane using Vitrobot Mark IV (Thermo Fischer Scientific). Cryo-
617 EM data collection was performed on a Titan Krios at 300 kV accelerating voltage in the Center
618 of Cryo-Electron Microscopy, Zhejiang University (Hangzhou, China). Micrographs were
619 recorded using a Gatan K2 Summit direct electron detector in counting mode with a nominal
620 magnification of 29,000 ×, corresponding to a pixel size of 1.014 Å. Image stacks was obtained
621 at a dose rate of about 8.0 electrons per $Å^2$ per second with a defocus ranging from -0.5 to -2.5
622 μm. The total exposure time was 8 s and intermediate frames were recorded in 0.2 s intervals,
623 resulting in an accumulated dose of 64 electrons per Å2 and a total of 40 frames per micrograph.
624 A total of 4740 and 4624 movies were collected for the antagonist bound $GABA_B$ heterodimer
625 and baclofen/BHFF bound–$GABA_B$–G_{i1} complex, respectively.

626

627 **Imaging processing and 3D reconstruction.**

628 For the dataset of antagonist-bound $GABA_B$ heterodimer, image stacks were subjected to beam-
629 induced motion correction using MotionCor2.1[54]. Contrast transfer function (CTF) parameters
630 for each non-dose weighted micrograph were determined by Gctf[55]. Semi-automated particle
631 selection were performed using RELION-3.0-beta2[56], yielded 2,969,413 particles. The particles
632 were extracted on a binned dataset with a pixel size of 2.028 Å and imported to CryoSPARC
633 v2.42[57] for 2 rounds of 2D classification. The poorly defined 2D classes were discarded,
634 producing 1,757,222 particles for further Ab-initio reconstruction and heterogeneous
635 refinement. After 2 rounds of heterogeneous refinement, the well-defined subset with 802,381
636 particles were re-extracted with a pixel size of 1.014 Å in Relion. The particles were
637 subsequently subjected to 3D classification, produced two good subsets accounting for 610,689
638 particles. Further 3D classifications focusing the alignment on the complex and the TMD
639 domains, produced high-quality subsets accounting for 374,595 particles, which were
640 subsequently subjected to 3D refinement and Bayesian polishing. The overall refinement
641 generated a map with an indicated global resolution of 3.0 Å at a Fourier shell correlation of
642 0.143. To further improve the map quality, local refinement focusing on the TMD and VFT
643 domains were performed in Relion. The locally refined map for the VFT and TMD show a
644 global resolution of 2.8 and 3.0 Å, which were merged using vop maximum command in UCSF
645 chimera[58]. This composite map was then 'Z-flip' to get the correct handedness and used for
646 subsequent model building and analysis.
647 For the dataset of $GABA_B$-G_{i1} complex, movies were subjected to beam-induced motion
648 correction using MotionCor2.1[54] and CTF estimation using Gctf[55]. Template-based automated
649 particle selection were performed using RELION-3.0-beta2, producing 3,075,533 particles for
650 further 2D classification in CryoSPARC. The well-defined classes with 1,471,649 particles
651 were selected for Ab-initio reconstruction and heterogeneous refinement, resulting in 488,801
652 particles with good density of the receptor. The subset was further re-extracted on a unbinned
653 dataset in Relion and performed multiple rounds of 3D classification. Three classes showed
654 different conformation of G protein binding (B1, B2a and B2b) were identified accounting for
655 30,542 particles, 130,901 particles and 16,048 particles, respectively. Whereas, other three
656 classes showed the fuzzy density of the G protein. Subsets for the 3 conformational states were

657 further subjected to 3D refinement and Bayesian polishing, yielded density maps with indicated
658 global resolutions of 8.8 Å, 6.8 Å, 8.6 Å, respectively. To find out the TMD conformations of
659 the G protein bound $GABA_B$, the map of dominant conformation, B2a, was further refined with
660 a mask on the receptor. The locally refined density map show a relatively clear density for the
661 TM bundle arrangement with an indicated resolution of 5.8 Å. Due to the highly consistency of
662 the receptor conformations in all 3D classes including three identified G protein-bound states
663 and three poorly defined G protein-bound classes, we reasoned that the receptor adopts the
664 same or highly similar conformation regardless of the orientation of G protein engagement. We
665 then focused the alignment on the receptor and performed 3D classification with a mask on the
666 receptor and TMD, respectively. The subsets accounting for 237,606 particles showed the high-
667 quality EM density were selected and were subjected to 3D refinement and Bayesian polishing.
668 The refinement generated a map with an indicated global resolution of 3.1 Å. To improve the
669 quality of TMD domain, local refinement focusing on the TMD and VFT domains were further
670 performed in Relion. The locally refined map for the VFT and TMD show a global resolution
671 of 2.8 and 3.2 Å, which were merged in UCSF chimera and used for subsequent model building
672 and analysis. Local resolution was determined using the Bsoft package[59] with half maps as input
673 maps.
674
675 **Model building and refinement**
676 The initial template of the TMDs in GB1 and GB2 was generated using SWISS-MODEL[60]. The
677 initial template of VFT domain was derived from the crystal structure of antagonist-bound
678 $GABA_B$ VFT (PDB 4MR7)[29]. Antagonist, agonist and PAM coordinates and geometry
679 restraints were generated using phenix.elbow[61]. Models of TMD and VFT domains were
680 docked into the EM density map of antagonist bound $GABA_B$ using UCSF Chimera[58]. The
681 initial model was subjected to iterative manual rebuilding in COOT[62] and real-space refinement
682 in PHENIX[61]. The final refinement statistics were validated using the module 'comprehensive
683 validation (cryo-EM)' in PHENIX. The refined model of antagonist-bound $GABA_B$ was used
684 as the initial model for baclofen/BHFF-bound $GABA_B$. Structures of TMD and VFT lobe
685 domains of GB1 and GB2 were docked into the density map using UCSF Chimera, respectively.

686 The model was further subjected to manual rebuilding and real-space refinement. The structures
687 of baclofen/BHFF-bound $GABA_B$ and G_{i1} protein from the structure of human cannabinoid
688 receptor 2-G_{i1} complex (PDB 6PT0)[63] were used to generate the docked model of $GABA_B$-G_i
689 complex in B1, B2a and B2b states, respectively. The refinement statistics of the inactive and
690 active $GABA_B$ heterodimer are provided in Table S1. Structure figures were created using
691 UCSF Chimera[58], and the UCSF Chimera X package[64].
692
693 **Data availability**
694 Cryo-EM maps have been deposited in the Electron Microscopy Data Bank under accession
695 codes: EMD-##### (CGP54626-bound $GABA_B$ receptor), EMD-##### (baclofen/BHFF-
696 bound $GABA_B$ in the presence of G_{i1} protein), EMD-##### ($GABA_B$-G_i complex in B1 state),
697 EMD-##### ($GABA_B$-G_i complex in B2a state) and EMD-##### ($GABA_B$-G_i complex in B2b
698 state). The atomic coordinates have been deposited in the Protein Data Bank under accession
699 codes: #### (CGP54626-bound $GABA_B$ receptor) and #### (baclofen/BHFF-bound $GABA_B$
700 in the presence of G_{i1} protein).
701
702

703 51 Milic, D. & Veprintsev, D. B. Large-scale production and protein engineering of G
704 protein-coupled receptors for structural studies. *Front Pharmacol* **6**, 66,
705 doi:10.3389/fphar.2015.00066 (2015).
706 52 Subedi, G. P., Johnson, R. W., Moniz, H. A., Moremen, K. W. & Barb, A. High Yield
707 Expression of Recombinant Human Proteins with the Transient Transfection of
708 HEK293 Cells in Suspension. *J Vis Exp*, e53568, doi:10.3791/53568 (2015).
709 53 Dror, R. O. *et al.* SIGNAL TRANSDUCTION. Structural basis for nucleotide
710 exchange in heterotrimeric G proteins. *Science (New York, N.Y.)* **348**, 1361-1365,
711 doi:10.1126/science.aaa5264 (2015).
712 54 Zheng, S. Q. *et al.* MotionCor2: anisotropic correction of beam-induced motion for
713 improved cryo-electron microscopy. *Nature methods* **14**, 331-332,
714 doi:10.1038/nmeth.4193 (2017).
715 55 Zhang, K. Gctf: Real-time CTF determination and correction. *Journal of structural*
716 *biology* **193**, 1-12, doi:10.1016/j.jsb.2015.11.003 (2016).
717 56 Scheres, S. H. Processing of Structurally Heterogeneous Cryo-EM Data in RELION.
718 *Methods in enzymology* **579**, 125-157, doi:10.1016/bs.mie.2016.04.012 (2016).
719 57 Punjani, A., Rubinstein, J. L., Fleet, D. J. & Brubaker, M. A. cryoSPARC: algorithms
720 for rapid unsupervised cryo-EM structure determination. *Nature methods* **14**, 290-296,
721 doi:10.1038/nmeth.4169 (2017).

58 Pettersen, E. F. *et al.* UCSF Chimera--a visualization system for exploratory research and analysis. *Journal of computational chemistry* **25**, 1605-1612, doi:10.1002/jcc.20084 (2004).

59 Heymann, J. B. Single particle reconstruction and validation using Bsoft for the map challenge. *Journal of structural biology* **204**, 90-95, doi:10.1016/j.jsb.2018.07.003 (2018).

60 Waterhouse, A. *et al.* SWISS-MODEL: homology modelling of protein structures and complexes. *Nucleic acids research* **46**, W296-w303, doi:10.1093/nar/gky427 (2018).

61 Adams, P. D. *et al.* PHENIX: a comprehensive Python-based system for macromolecular structure solution. *Acta crystallographica. Section D, Biological crystallography* **66**, 213-221, doi:10.1107/s0907444909052925 (2010).

62 Emsley, P. & Cowtan, K. Coot: model-building tools for molecular graphics. *Acta crystallographica. Section D, Biological crystallography* **60**, 2126-2132, doi:10.1107/s0907444904019158 (2004).

63 Xing, C. *et al.* Cryo-EM Structure of the Human Cannabinoid Receptor CB2-Gi Signaling Complex. *Cell* **180**, 645-654.e613, doi:10.1016/j.cell.2020.01.007 (2020).

64 Goddard, T. D. *et al.* UCSF ChimeraX: Meeting modern challenges in visualization and analysis. *Protein science : a publication of the Protein Society* **27**, 14-25, doi:10.1002/pro.3235 (2018).

Figure 1

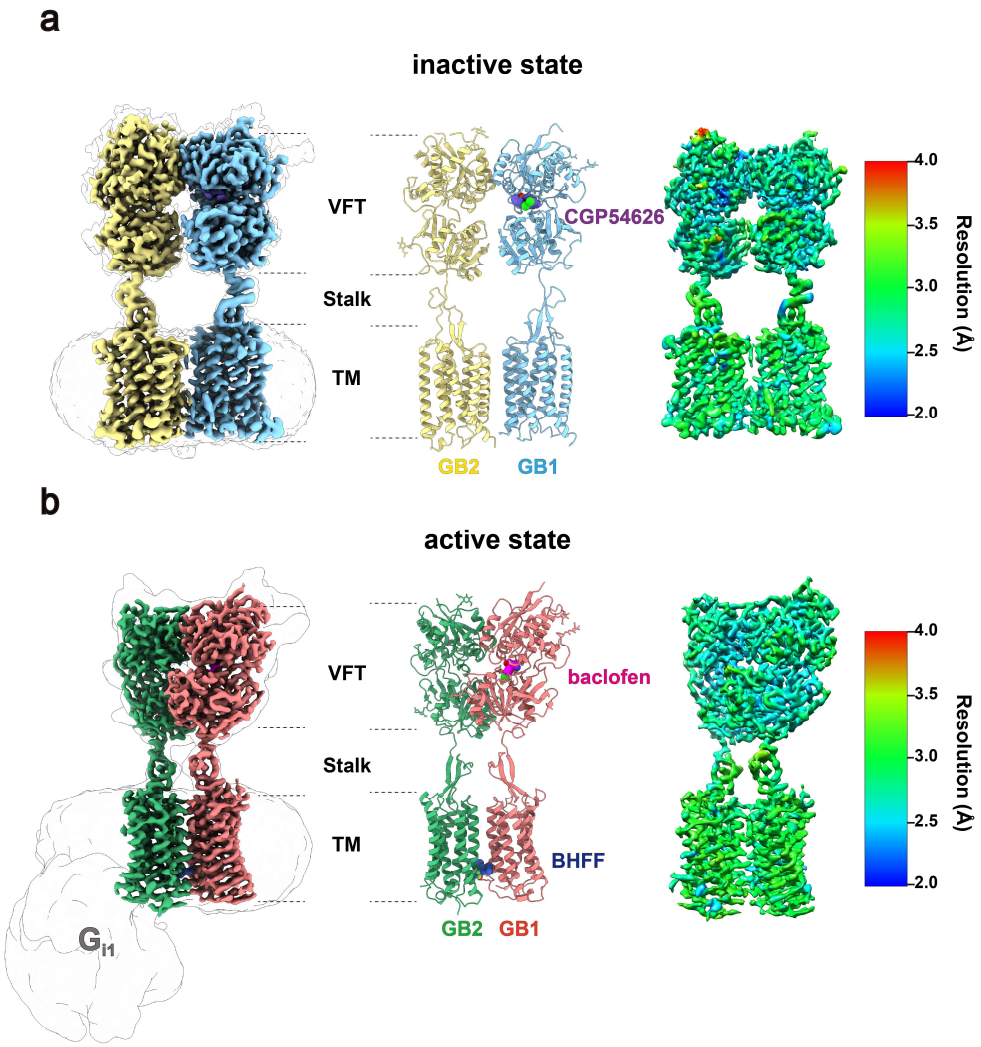

Fig.1 | Cryo-EM structures of $GABA_B$ receptor in the inactive and active states. a-b, Cryo-EM density maps (left), models (middle) and maps coloured according to local resolution (right) for the $GABA_B$ receptor in the presence of CGP54626 (slate; antagonist) (**a**) and in complex with baclofen (magenta; agonist), BHFF (steel blue; PAM) and G_{i1} protein (**b**). The coloured density map is a composite map generated with the VFT and TMD locally refined map. The cryo-EM density map before focused refinement in transparent superposed with the final map, illustrating density for detergent micelle and G_{i1} protein. The local resolution (Å) was calculated with the locally refined map as input, indicating a range of 2.5-3.5 Å resolution in most map regions for both the inactive and active states. GB1 and GB2 in inactive state, blue and yellow, respectively; red and green in active state, respectively.

Figure 2

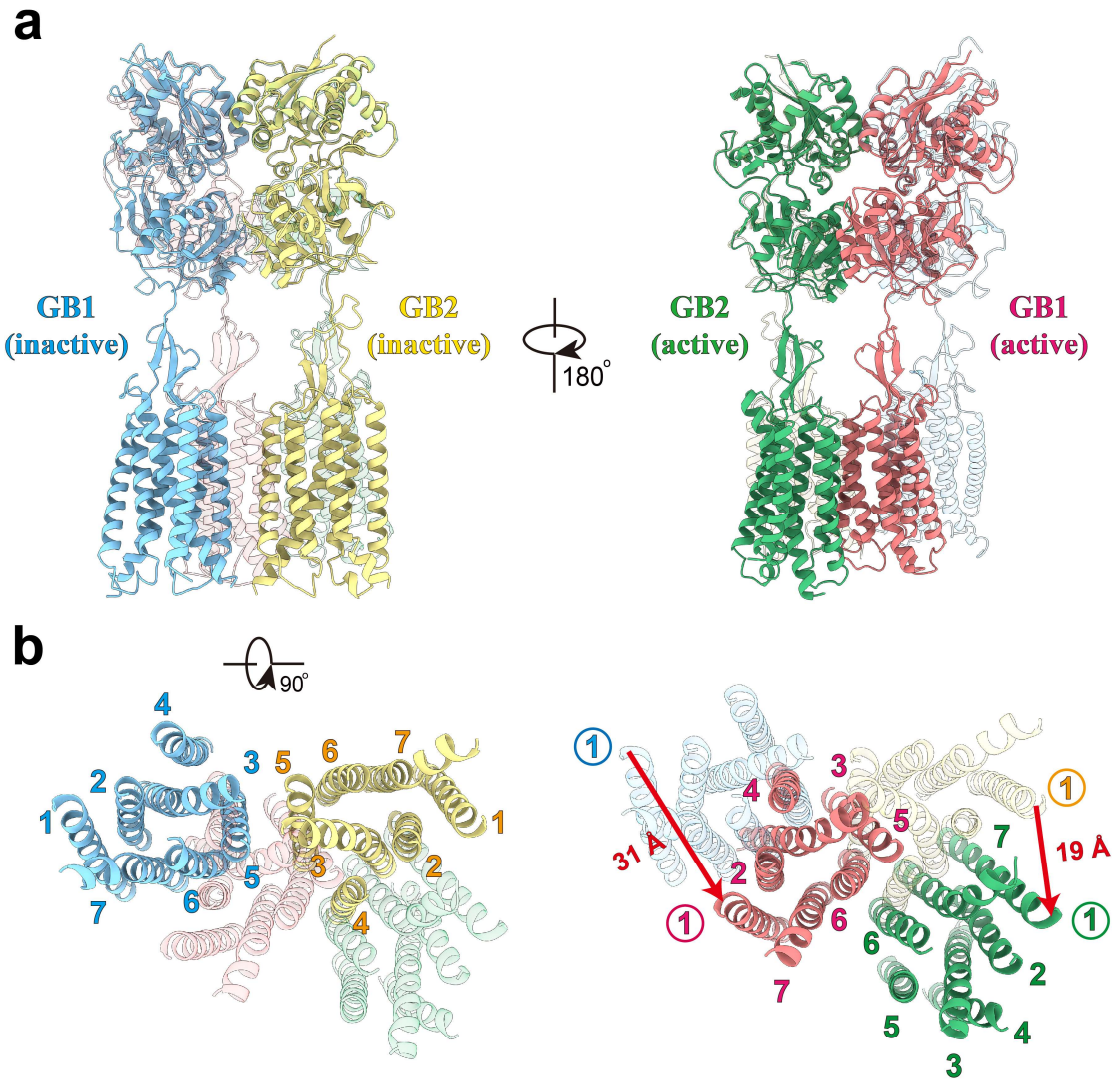

Fig.2 | Structural comparison of GABAB receptor in inactive and active states. a-b, Orthogonal views of the superimposed structures of $GABA_B$ receptor in inactive and active states, showing the domain repositioning upon agonist binding induced activation. Side views (**a**) and intracellular views (**b**) of superposed structures are shown, with the active structure in translucent in the left panels and the inactive structure in translucent in the right panels, respectively. VFT domains and loops are omitted for clarity in **b**. Red arrows indicate the translation direction and distance for GB1 and GB2 (measured at extracellular tips of TM1 helices), respectively. Structures were aligned on the combined domains of GB1 VFT and GB2 lobe1, the relatively stable parts of the receptor along activation pathway.

Figure 3

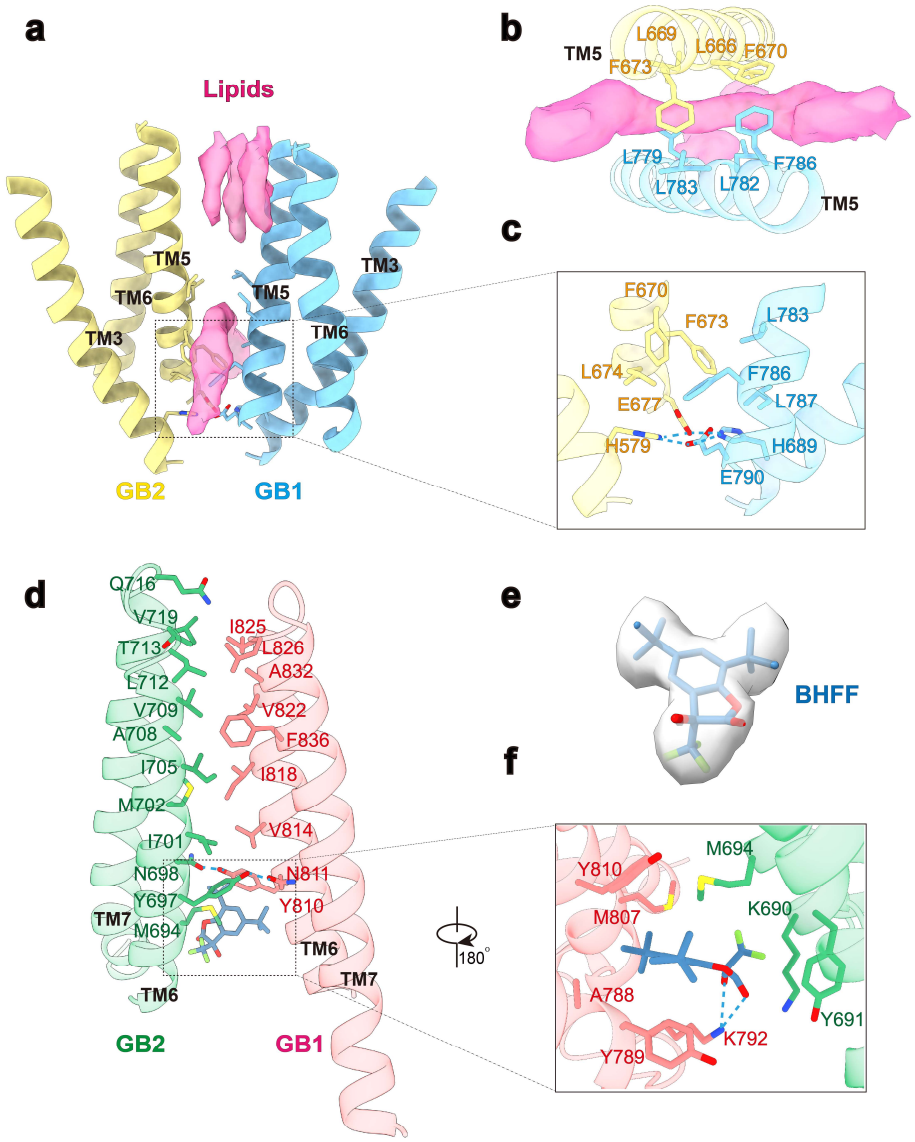

Fig.3 | Structural details of the TM heterodimeric interfaces for the inactive and active $GABA_B$ structures. a-b, Side (**a**) and intracellular (**b**) views of the inactive TM interface. EM densities (magenta) corresponding to putative cholesterols are shown in surface. **c**, close view of inactive TM interface in the proximal to the cytoplasm. $H689^{3.55}$ and $E790^{5.60}$ of GB1, $H579^{3.55}$ and $E677^{5.60}$ of GB2 forms salt bridge network to stabilize an inactive conformation. **d**, Detailed interactions of the TM interface in active state. **e-f**, Cryo-EM density (**e**) and the detailed interactions (**f**) of (+)-BHFF (PAM) in the active TM interface. The critical residues are shown as sticks. Hydrogen bonds are depicted as dashed lines.

Figure 4

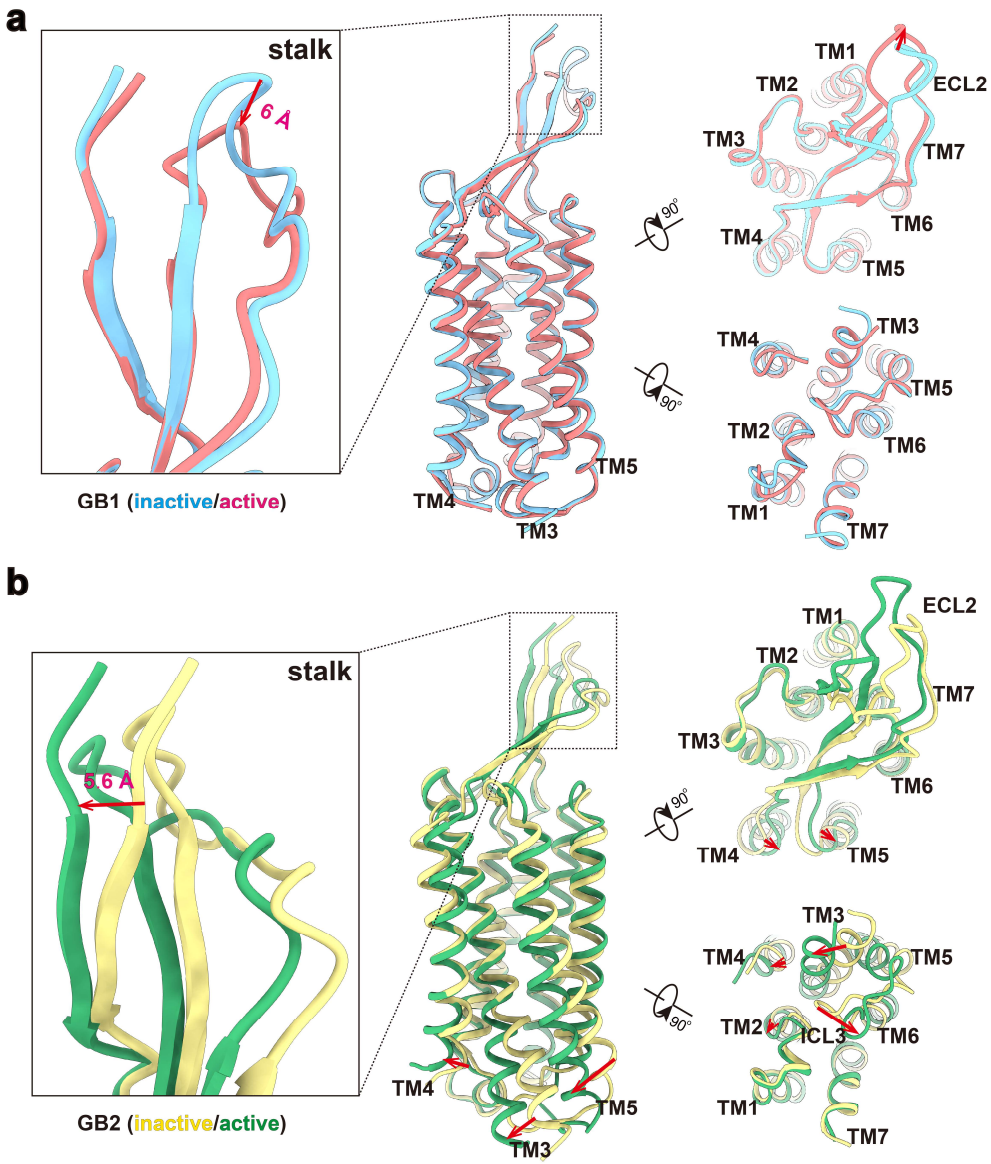

Fig.4 | Structural comparison of individual TM domains between inactive and active states. GB1 TM domain (**a**) and GB2 TM domain (**b**) between inactive and active states are superposed respectively. Side, extracellular and intracellular views are shown. Magnified views of the stalk domains are shown in the left. Red arrows represent the movement direction and distance of TMs and loops.

Figure 5

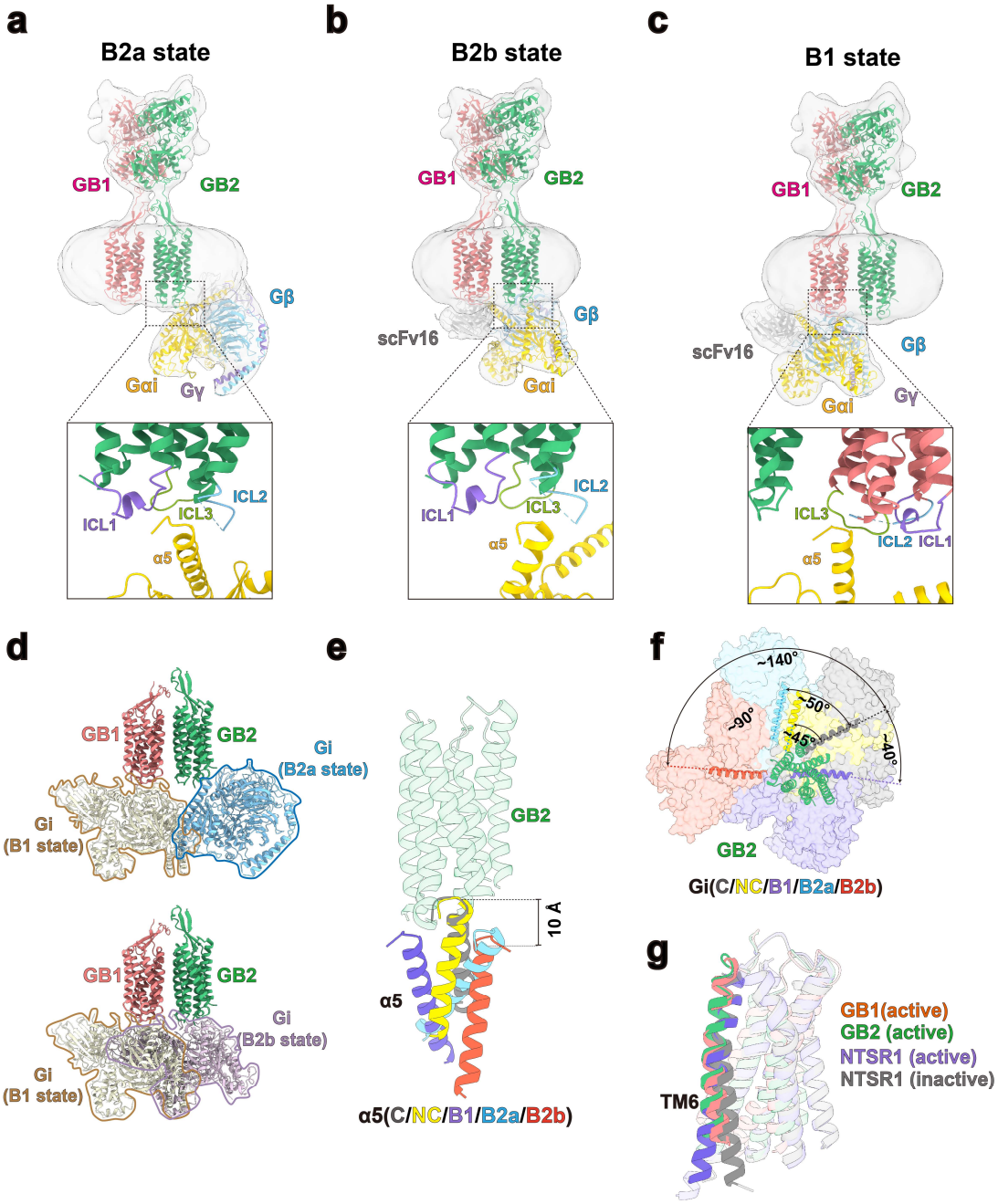

Fig.5 | Three distinct modes of Gi coupling to $GABA_B$ receptor. a-c, Cryo-EM density maps and the models of the $GABA_B$–G_{i1} complex in B2a state (**a**), B2b state (**b**), and B1 state (**c**). Magnified views of the interaction between α5-helix of Gαi and $GABA_B$ receptor are shown in the bottom. GB1 in red, GB2 in green, Gαi in gold, Gβ in cyan, Gγ in purple and scFv16 in grey. Intracellular loops 1, 2, and 3 are highlighted. **d**, Superposition of the B1 state with either B2a state or B2b state showing the potential steric clash between Gi proteins, indicating that only one Gi protein can bind to $GABA_B$ receptor at one time. Gi in

B2a state, brown; Gi in B2b state, blue; Gi in B1 state, grey. **e**, Comparison of the $G\alpha_{i1}$ α5-helix binding position between GB1 (B1 state), GB2 (B2a and GB2b states) and the NTSR1–Gi1 protein complex in canonical (C; PDB code: 6OS9) and noncanonical (NC; PDB code: 6OSA) states. The position of α5-helix from $GABA_B$–Gi complex in different states show around 10 Å downward movement compared with that of NTSR1–G_{i1} complex. Structures were aligned by the TM domains and only GB2 TM domain is shown for clarity. Color usage for α5: C state, grey; NC state, gold; B1 state, purple; B2a state, cyan; and B2b state, red. **f**, Orientations of the Gi protein when coupling to $GABA_B$ and NTSR1 receptors. Rotation of Gi protein are measured by the αN domains. G proteins are coloured as described in **e**. **g**, Comparison of the active GB1 and GB2 TM domains with the inactive and active structures of NTSR1, showing the positions of TM6 helices of GB1 and GB2 subunits are similar to that of NTSR1 in inactive state.

Extended Data Figure 1

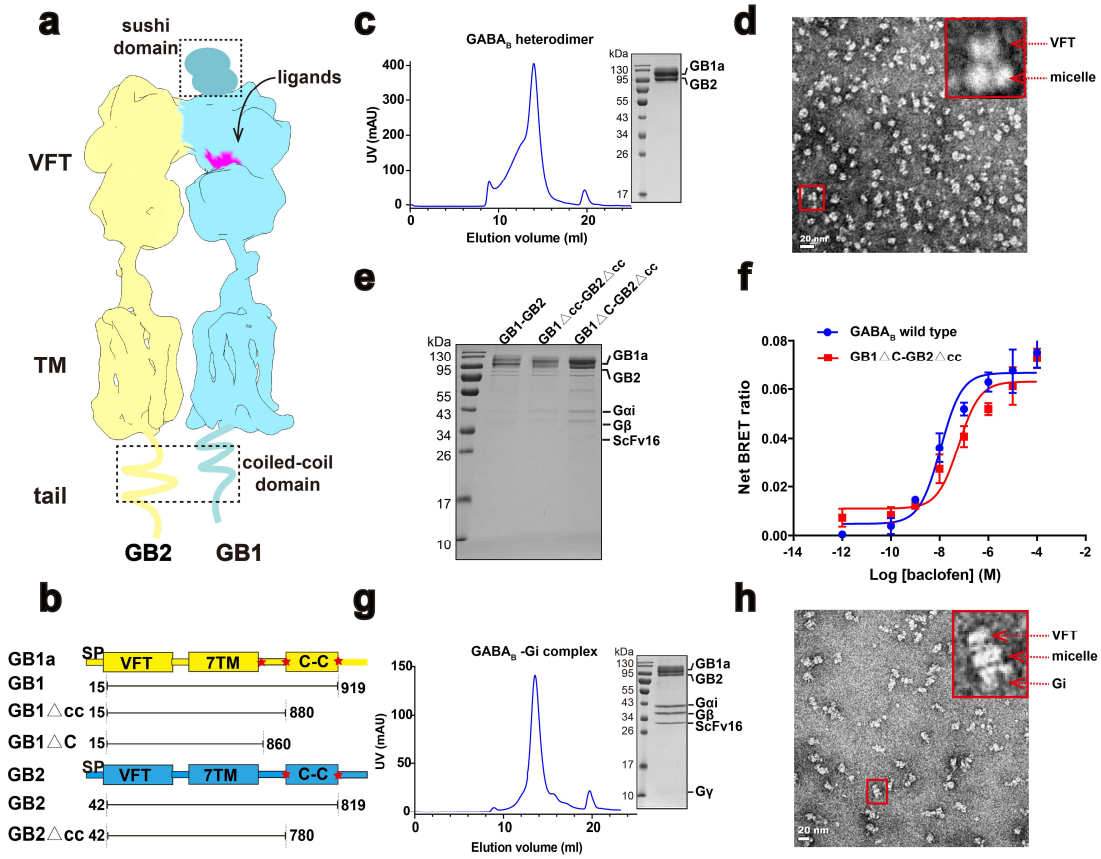

Extended Data Fig.1 | Purification and characterization of the GABA$_B$ heterodimer and GABA$_B$–G$_{i1}$ complex. a, Schematic of the heterodimeric GABA$_B$ receptor. **b,** Schematic of constructs used in this study. △cc represents the coiled-coil (c-c) domain is removed. △C represents the entire C-terminus after TM domain in GB1 or GB2 is truncated. **c**, Size-exclusion chromatography profile and SDS-PAGE gel of the purified antagonist-bound GABA$_B$ receptor. **d**, Negative staining EM analysis of the purified inactive GABA$_B$ receptor shows the clear density for VFT and detergent micelles. **e**, G protein pull-down analysis of the different truncations (GB1-GB2, GB1△cc-GB2△cc, and GB1△C-GB2△cc) of GABA$_B$ receptor. SDS-PAGE gel showed that GB1△C-GB2△cc exhibits a greater efficiency in complex formation among these constructs and were selected for further structural study. **f**, Dose-response curve of baclofen-induced BRET changes in the Gαi sensors for the wide-type and GB1△C-GB2△cc construct of GABA$_B$ receptor, showing that GB1△C-GB2△cc exhibits similar phrenology to that of wild-type receptor. **g**, Size-exclusion chromatography profile and SDS-PAGE gel of the purified agonist/PAM bound GABA$_B$–G$_{i1}$ complex using GB1△C-GB2△cc construct. **h**, Negative staining EM visualization of the purified GABA$_B$-G$_{i1}$ complex showing clear density for VFT, detergent micelles and G$_{i1}$ protein.

Extended Data Figure 2

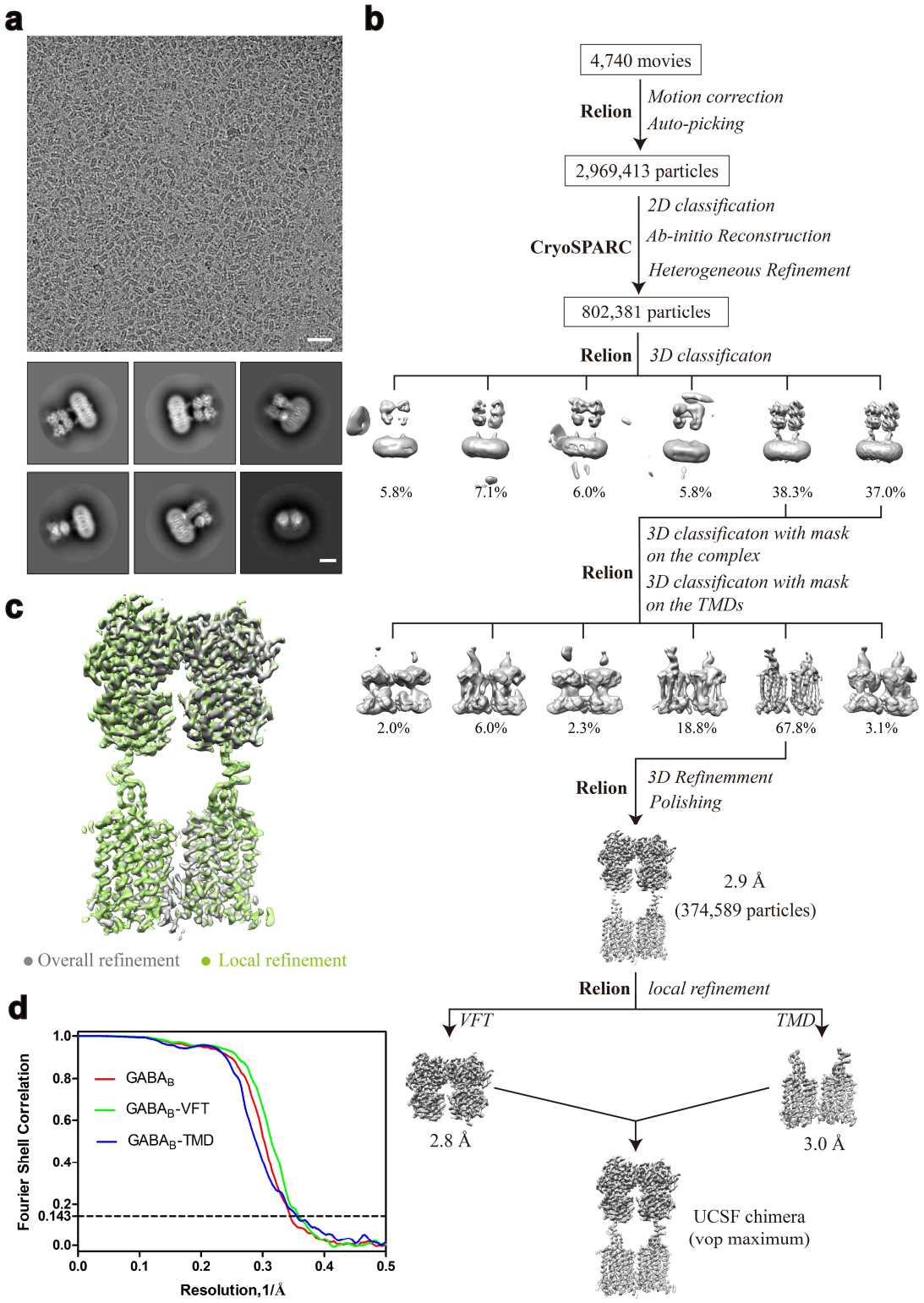

Extended Data Fig.2 | Single-particle cryo-EM of the CGP54626-bound GABA$_B$ receptor. a, Cryo-EM micrograph (scale bar: 30 nm) and representative two-dimensional class averages of the inactive GABA$_B$ receptor in LMNG detergent micelles (scale bar: 5 nm). **b**, Flow chart of cryo-EM data processing. Details are described in Method section. **c**, Comparison of the overall refined map and the locally

refined composite map. The locally refined composite map exhibits a slight improvement of the TMs density and adopts almost the identical conformation with the overall refined map. **d**, Gold-standard Fourier shell correlation (FSC) curves of overall refined receptor and the locally refined VFT and TMD.

Extended Data Figure 3

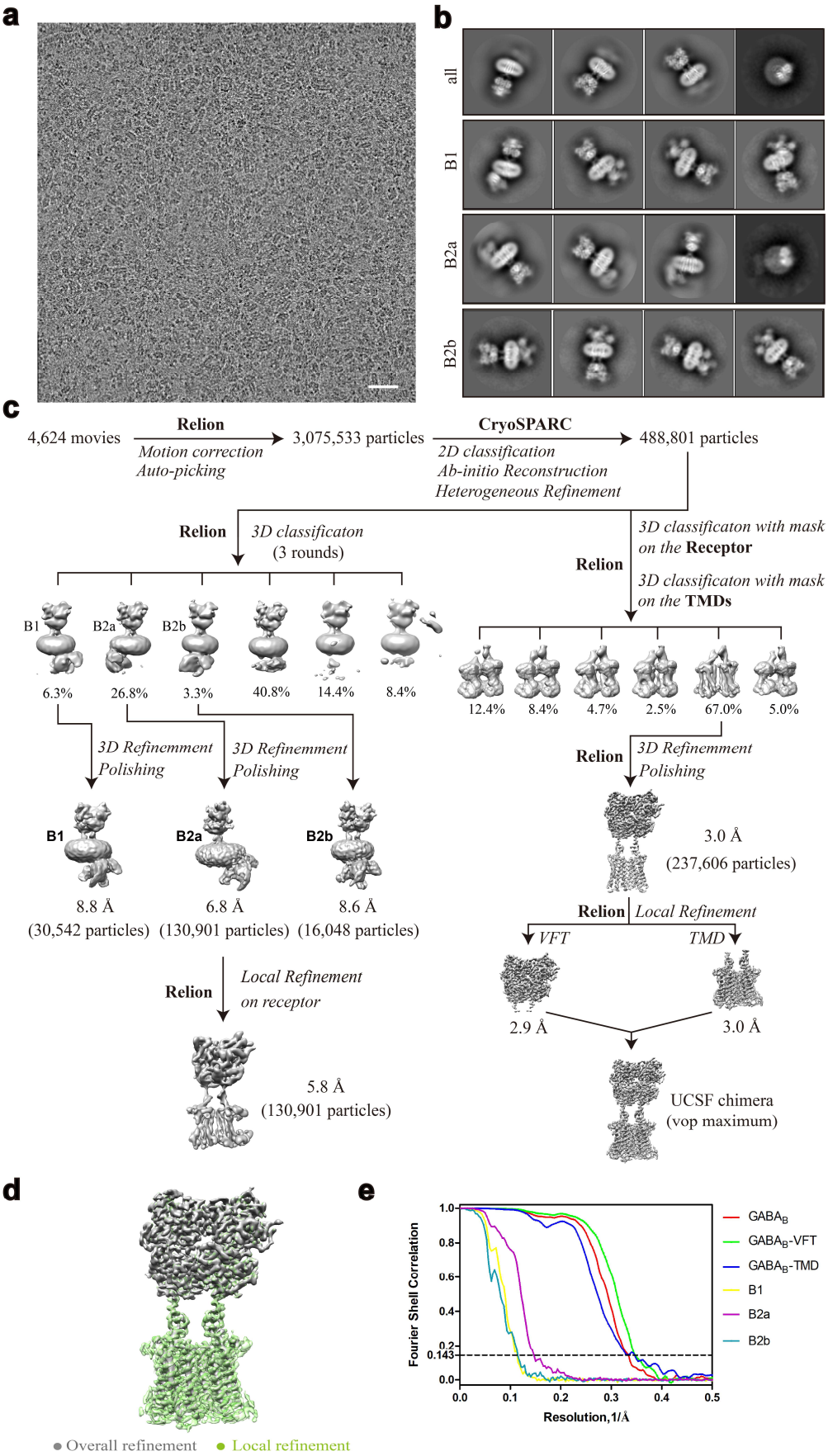

Extended Data Fig.3 | Single-particle reconstruction of the agonist/PAM-bound $GABA_B$–G_{i1} complex. a, Representative cryo-EM micrograph of the $GABA_B$–G_{i1} complex (scale bar: 30 nm). **b**, Representative two-dimensional class averages of the overall refined $GABA_B$ receptor (all) and the $GABA_B$–G_{i1} complex in B1, B2a and B2b states, respectively. (scale bar: 5 nm). **c**, Flow chart of cryo-EM data processing. Details are described in method section. **d**, Comparison of the overall refined map and the locally refined composite map. The locally refined composite map shows a substantial improvement for the TM density and exhibits almost the same conformation with the overall refined map. **e**, Gold-standard Fourier shell correlation curves of overall refined receptor, the locally refined VFT and TMD and the refined $GABA_B$-G_{i1} complex in B1, B2a, B2b states.

Extended Data Figure 4

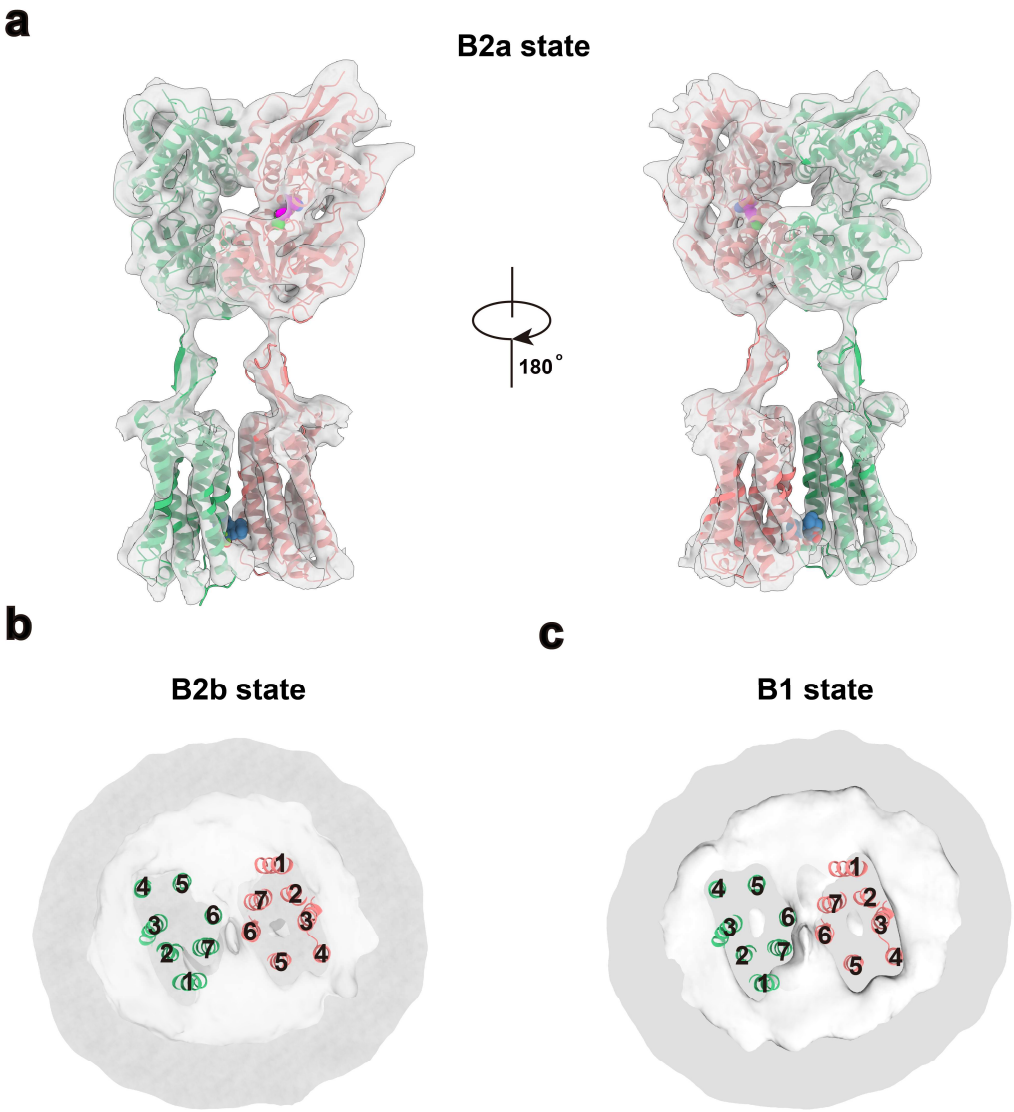

Extended Data Fig.4 | Fitting of the active $GABA_B$ structure into the cryo-EM density maps of $GABA_B$–G_{i1} complex in B2a, B2b and B1 states. a, Side views of the active $GABA_B$ structure derived from the high-resolution density map against cryo-EM map of $GABA_B$–G_{i1} complex in B2a state. **b-c**, Cut through of bottom-up views of the active $GABA_B$ structure derived from the high-resolution density map against cryo-EM map of $GABA_B$–G_{i1} complex in B2b state (**b**) and B1 state (**c**), respectively. The model of $GABA_B$ receptor was rigid-body docked into the density.

Extended Data Figure 5

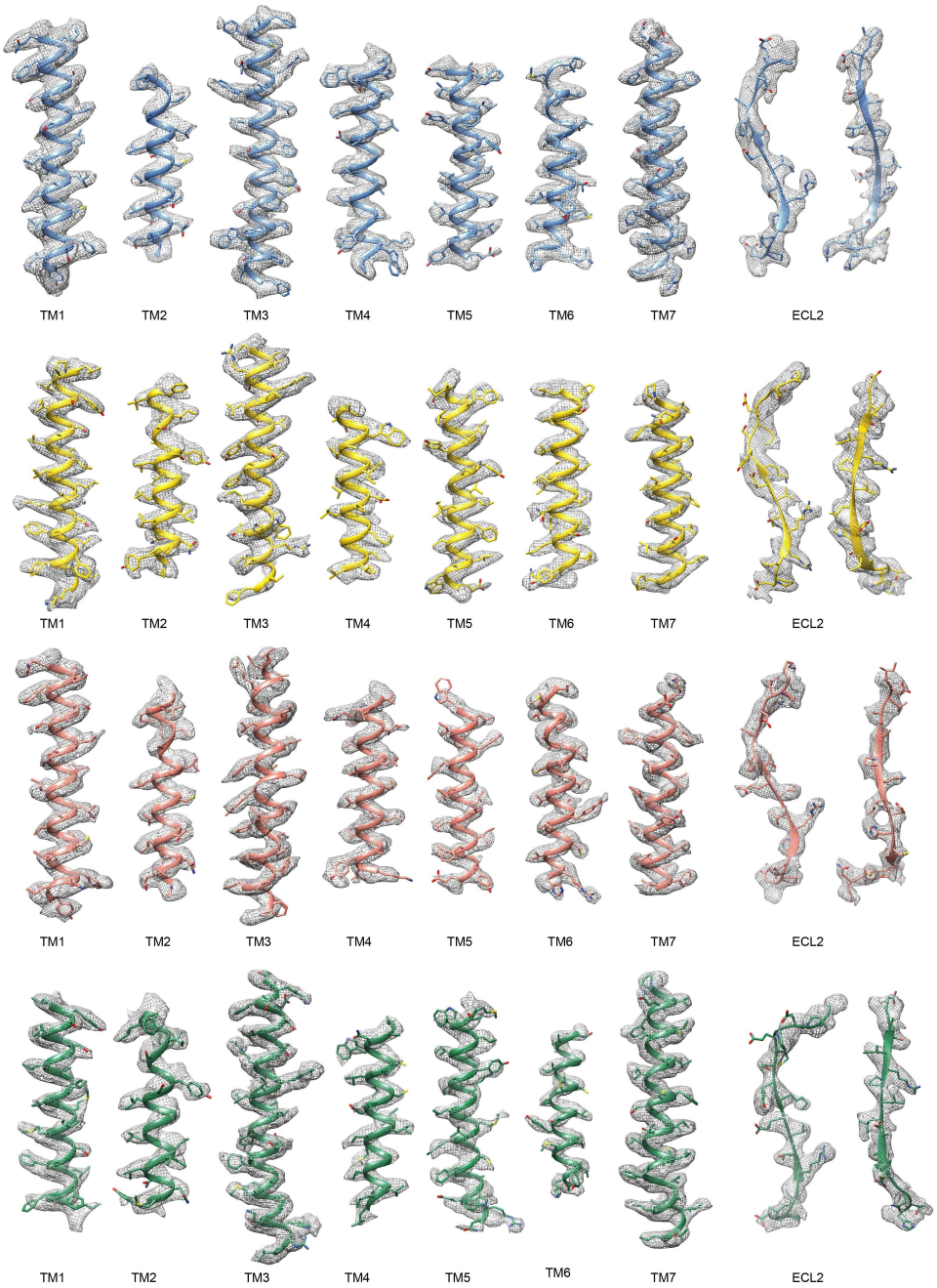

Extended Data Fig.5 | Electron density of transmembrane helices and ECL2 in $GABA_B$ receptor. Cryo-EM density of transmembrane helices of $GABA_B$ in inactive and active structures. Inactive GB1 in blue; Inactive GB2 in yellow; Active GB1 in red; Active GB2 in green.

Extended Data Figure 6

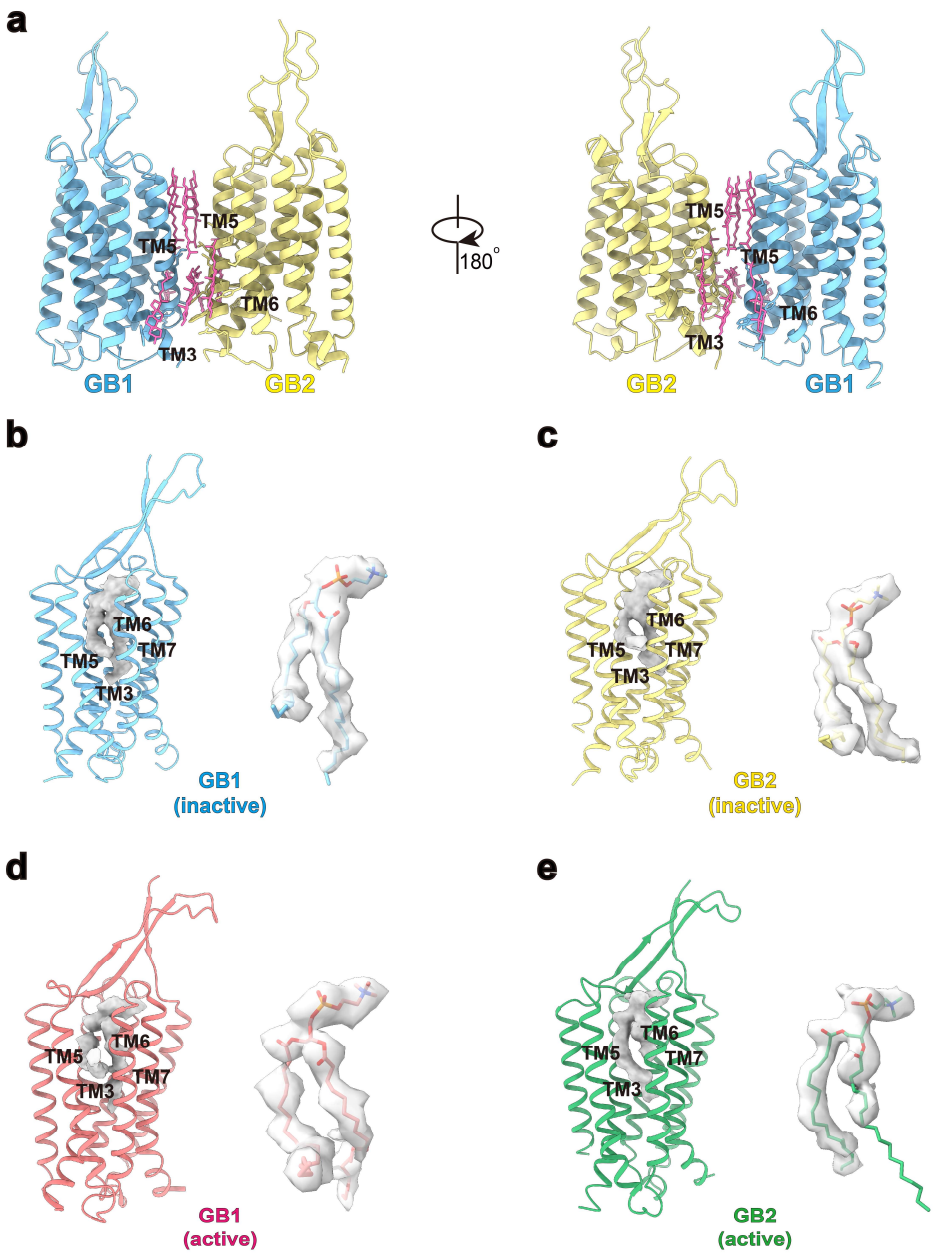

Extended Data Fig.6 | Putative cholesterols and phospholipids in $GABA_B$ receptor. **a**, The putative cholesterols between the inactive TM interface are shown. **b-e**, Phospholipid-like densities inside the TM bundles of inactive and active $GABA_B$ structures. Fitting of the phosphatidylcholine, the most abundant phospholipid in mammalian cells, into the unassigned densities in inactive and active structures. The buried surface area of each phospholipid in inactive GB1(**a**), inactive GB2 (**b**), active GB1 (**c**) and active GB2 (**d**) is 1377 $Å^2$, 1294 $Å^2$, 1361 $Å^2$, 1365 $Å^2$, respectively. Inactive GB1 in blue; Inactive GB2 in yellow; Active GB1 in red; Active GB2 in green.

Extended Data Figure 7

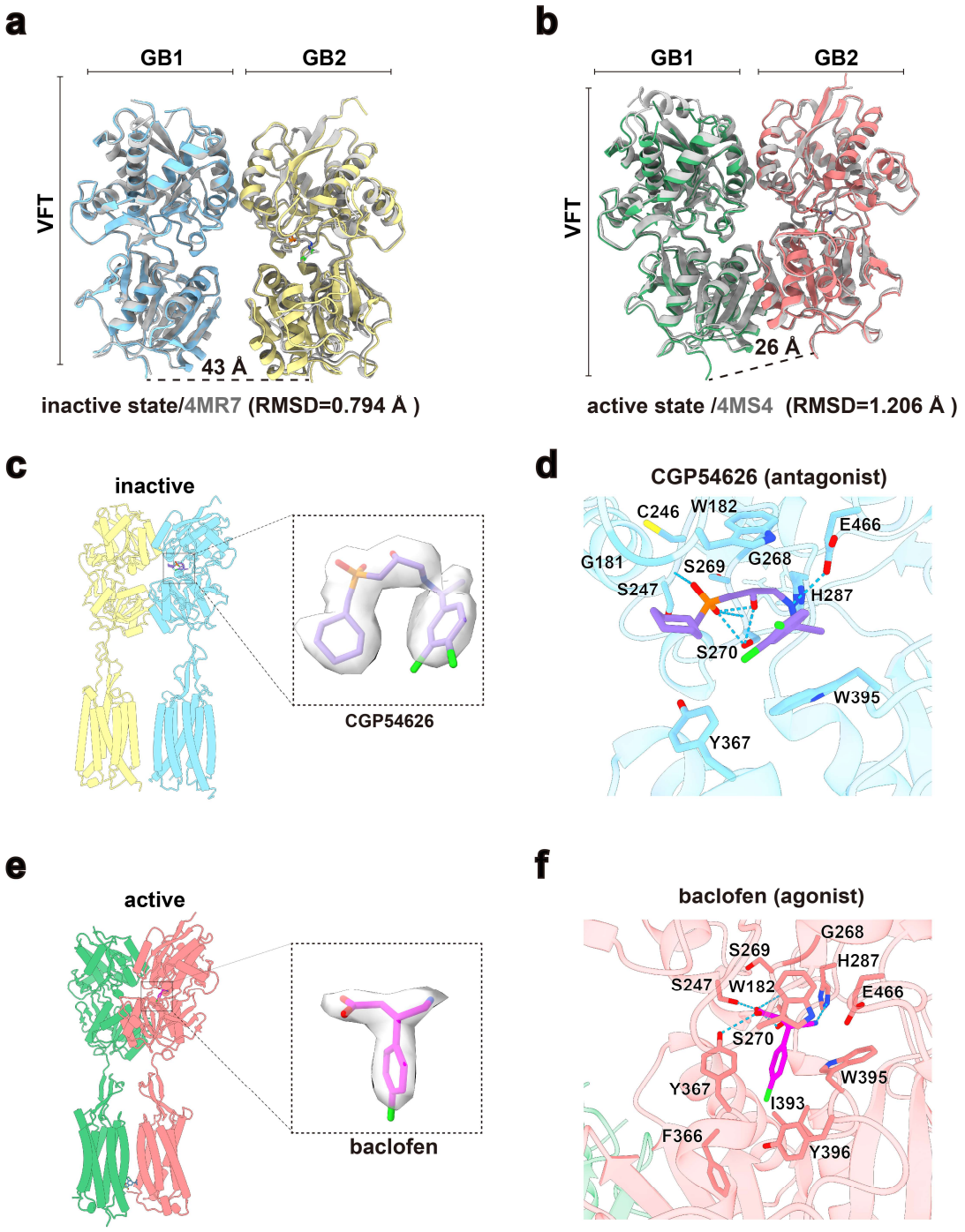

Extended Data Fig.7 | Structural comparisons of the VFT and ligand binding site. **a**, Superimposition of VFT domain from inactive structure of full-length $GABA_B$ receptor and crystal structure of CGP54626-bound soluble VFT domain (grey; PDB code: 4MR7). **b**, Superimposition of VFT domain from active structure of full-length $GABA_B$ receptor and crystal structure of baclofen-bound soluble VFT domain (grey; PDB code: 4MS4). **c-d**, Cryo-EM density (**c**) and the binding pocket analysis (**d**) of CGP54626 in inactive state. Detailed interaction of CGP54626 in the orthosteric

binding site, in agreement with the reported crystal structure of CGP54626-bound $GABA_B$ VFT. **e-f**, Cryo-EM density (**e**) and the binding pocket analysis (**f**) of baclofen in active state. Detailed interaction of baclofen in the orthosteric binding site is in agreement with the reported crystal structure of baclofen-bound $GABA_B$ VFT.

Extended Data Figure 8

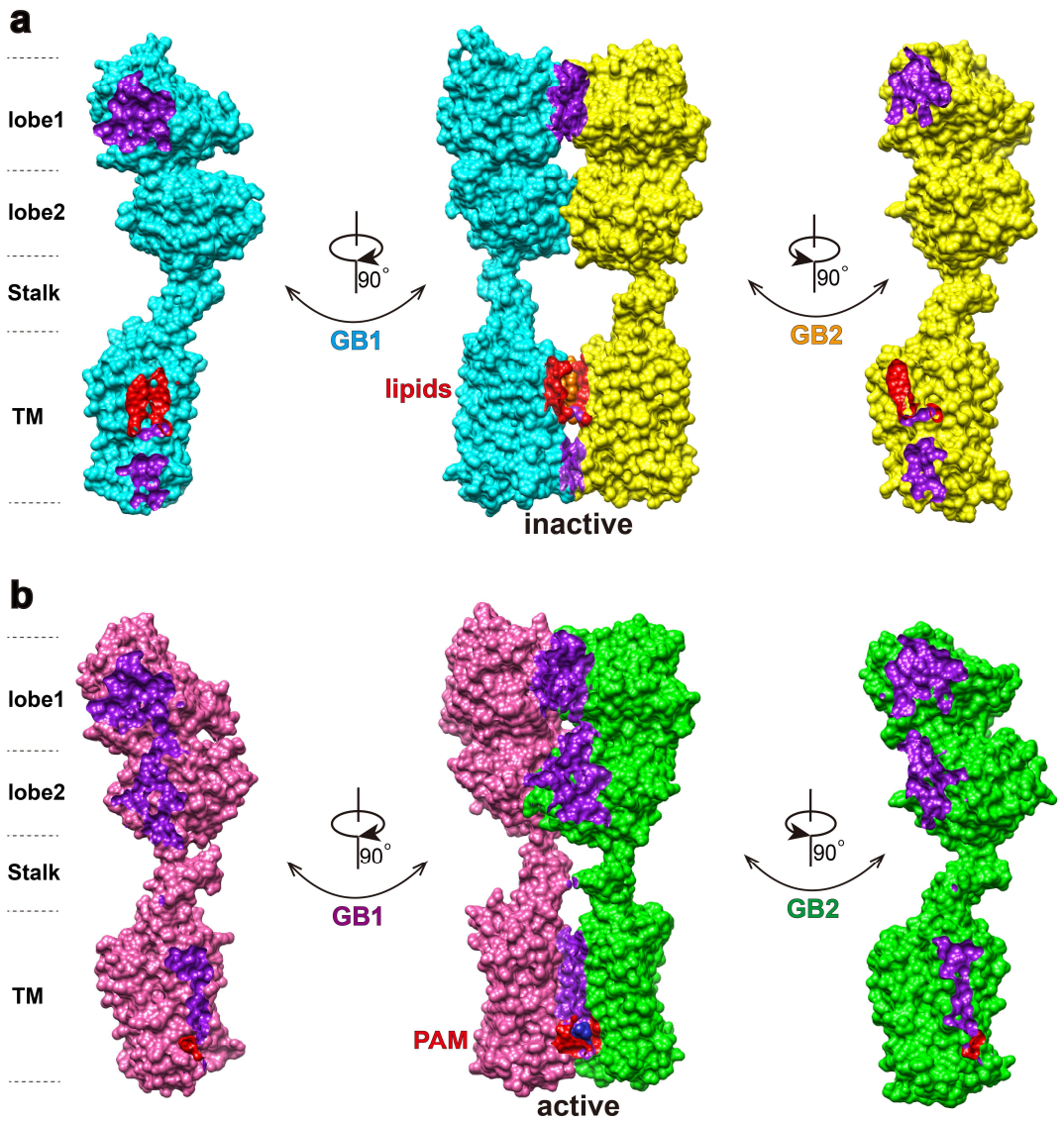

Extended Data Fig.8 | Comparison of the intersubunit interfaces in inactive and active GABA$_B$ receptor. Intersubunit interfaces in inactive (**a**) and active (**b**) GABA$_B$ receptor. The direct interface of GB1 and GB2 are colored purple. The putative cholesterols and the PAM interfaces are colored red.

Extended Data Figure 9

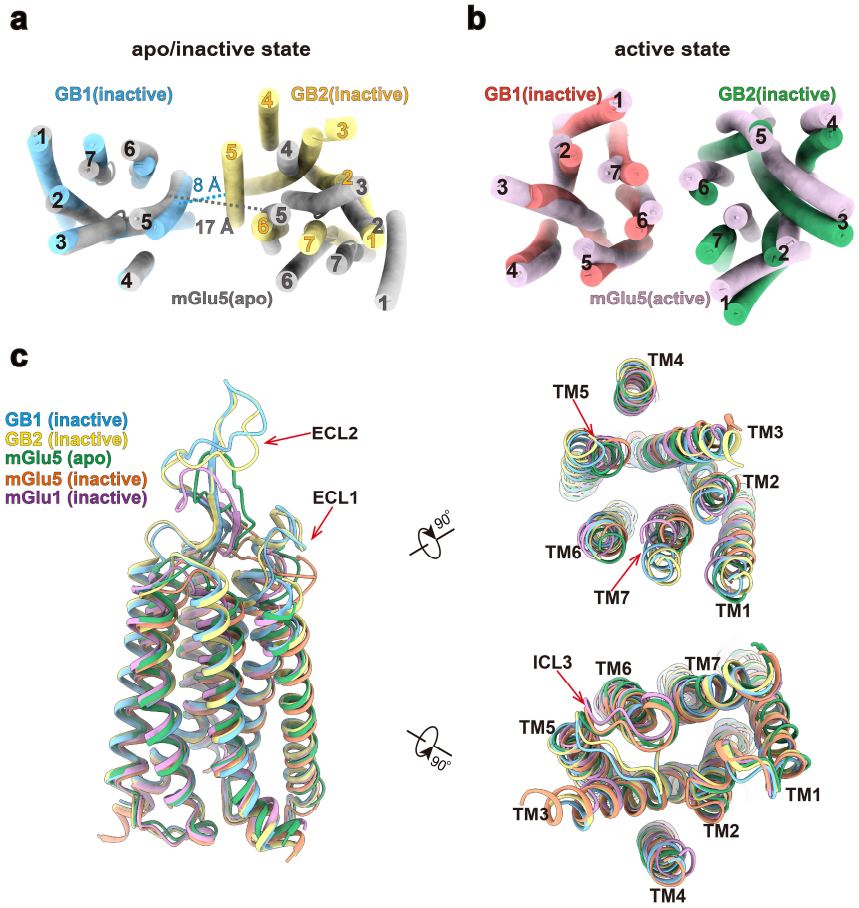

Extended Data Fig.9 | Structural comparison of GABA$_B$ with mGlu receptors. a-b, Extracellular view of the superposed TM bundles of GABA$_B$ and mGlu5 in inactive apo state (grey; PDB code: 6N52) (**a**) and active state (pink; PDB code: 6N51) (**b**). The TM5 helices of GABA$_B$ receptor are closer compared with that of the inactive mGlu5 receptor measured at the closest separation of TM5 helices. **c**, Superimposition of TM domains of inactive GABA$_B$ receptor, inactive mGlu1 (PDB code: 4or2) and inactive, apo mGlu5 (PDB code: 4oo9, 6N52). Red arrow represents the conformational difference of TM5, TM7, ECL1, ECL2, ICL3 between the GABA$_B$ and the mGlu receptors.

Extended Data Figure 10

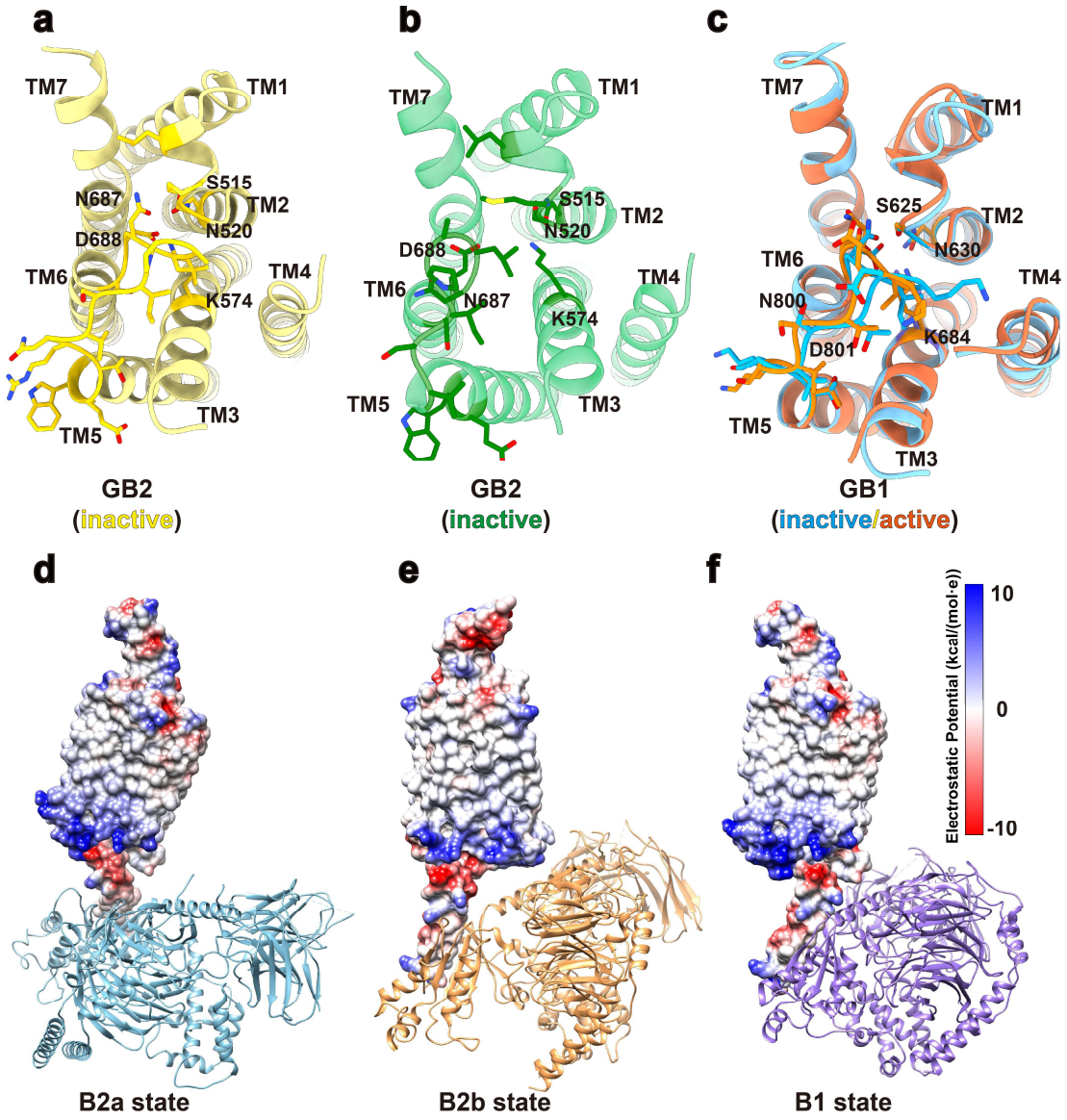

Extended Data Fig.10 | Conformation of ICL3 in inactive and active $GABA_B$ structures and the α5–receptor interface in $GABA_B$–G_{il} complex. a-c, Interactions of the ICL3 with other residues of TM domain in GB2 inactive (**a**), active state(**b**) and GB1 in both states(**c**). **d-f**, Electrostatic charge surface illustrating the interface of with the $GABA_B$ receptor in B2a (**d**), B2b (**e**)and B1(**f**) states, showing the complementary-charge distribution between the C terminus of the α5-helix and the cytoplasmic surface of TM bundle.

Extended Data Table 1

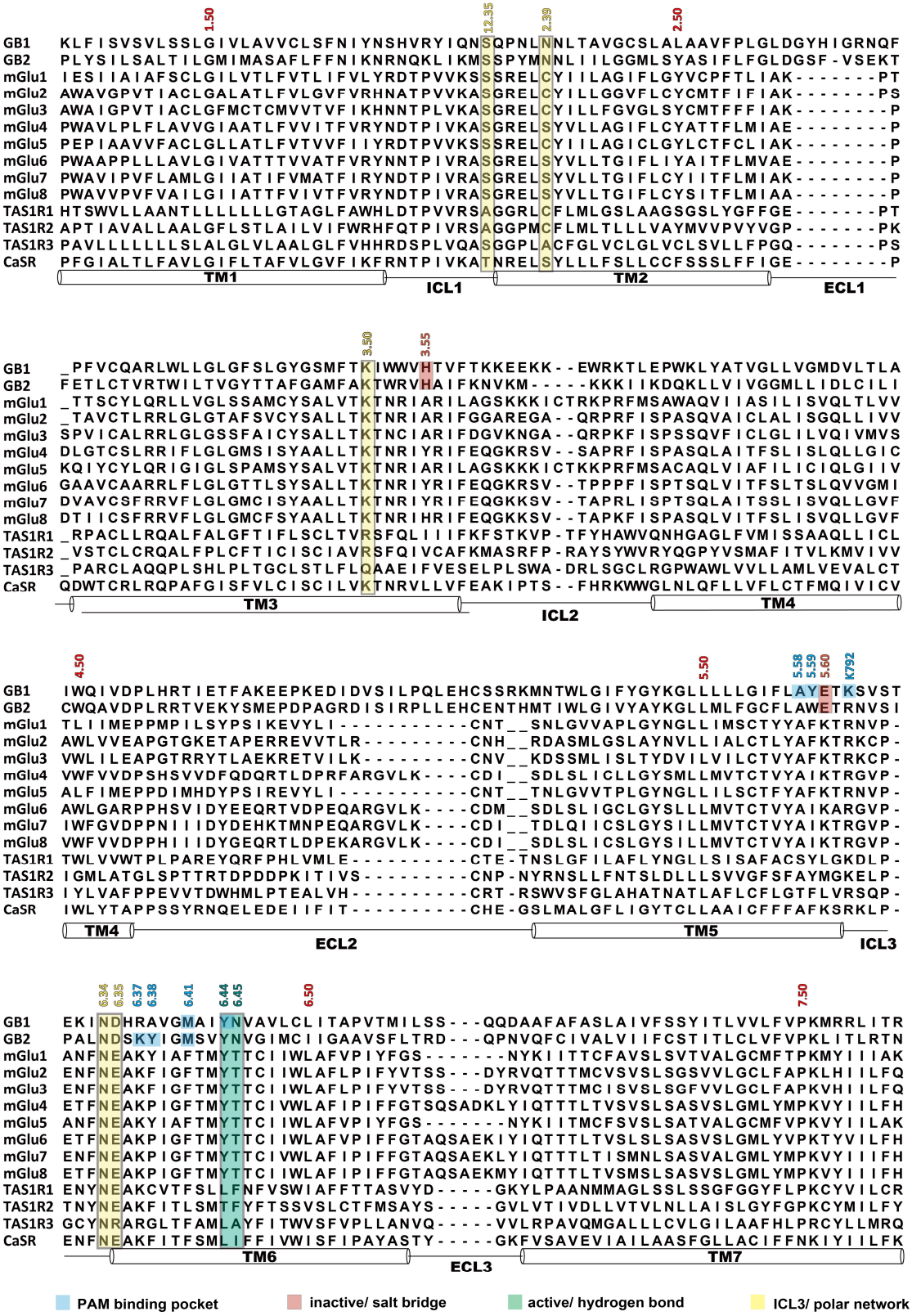

Extended Data Table 1 | Sequence alignment of TMs of class C GPCRs.

The sequence alignment of TMs of class C GPCRs was created using GPCRdb (http://www.gpcrdb.org) and Jalview software. Secondary structure elements are

annotated underneath the sequences. Highlighted are residues involved in PAM binding pocket (blue), salt bridge in inactive TM interface, hydrogen bond in active TM interface (green) and polar network stabilizing ICL3 (yellow).

Extended Data Table 2
Cryo-EM data collection, refinement and validation statistics

	Inactive $GABA_B$ receptor	Active $GABA_B$ receptor
Data collection and processing		
Magnification	4,9310	4,9310
Voltage (kV)	300	300
Electron exposure (e–/Å^2)	62	62
Defocus range (μm)	-0.5 ~ -2.5	-0.5 ~ -2.5
Pixel size (Å)	1.014	1.014
Symmetry imposed	C1	C1
Initial particle images (no.)	2,969,413	3,075,533
Final particle images (no.)	374,589	237,606
Map resolution (Å)		
(Overall/VFT/TM)	2.9/2.8/3.0	3.0/2.9/3.0
FSC threshold	0.143	0.143
Map resolution range (Å)	2.2-4.0	2.2-4.0
Refinement		
Initial model used (PDB code)	4MR7	inactive $GABA_B$ structure
Model resolution (Å)	2.9	3.3
FSC threshold	0.5	0.5
Model resolution range (Å)	2.5-4.0	2.5-4.0
Map sharpening *B* factor (Å^2)		
(Overall/VFT/TM)	83.6/84.1/67.6	78.5/80.9/190.3
Model composition		
Non-hydrogen atoms	10915	10894
Protein residues	1355	1348
Ligands	9	10
B factors (Å^2)		
Protein	61.64	66.88
Ligand	63.76	88.08
R.m.s. deviations		
Bond lengths (Å)	0.006	0.004
Bond angles (°)	0.741	0.684
Validation		
MolProbity score	1.69	1.65
Clashscore	8.01	7.15
Poor rotamers (%)	0.00	0.00
Ramachandran plot		
Favored (%)	96.27	96.18
Allowed (%)	3.73	3.82
Disallowed (%)	0.00	0.00